RIMS Kôkyûroku Bessatsu
B52 (2014), 11–53

On the geometric aspect of Sato's postulates on the S-matrix

Dedicated to Professor Takashi Aoki on his sixtieth birthday,
who has been effectively employing a computer in the exact WKB analysis

By

Naofumi HONDA[*], Takahiro KAWAI[**] and Henry P. STAPP[***]

Abstract

We study the singularity structure of the Landau-Nakanishi surface determined by a hooked 3-lines diagram, and this gives a new light on Sato's postulates on the S-matrix.

§ 1. Introduction

This paper is the first step of our trial to cast a new light on Sato's postulates ([11]) on the singularity structure of the S-matrix by assuming the Borel summability ([2]) of its perturbation series expansion in the coupling constant. In this paper we put our emphasis on the study of its geometric aspect, particularly near its three particle threshold (hereafter abbreviated as $3PT$). In order to make our study concrete and simple, we assume that the space-time dimension is 2 and that all the masses associated with internal lines are equal to m ($\gneq 0$), and, having the 3 to 3 S-matrix element in mind, we investigate, with the help of a computer, the concrete shape of the *positive-α Landau-Nakanishi surface* determined by a *hooked 3-lines diagram*, whose definition is given in Section 2.

Received March 24, 2014. Revised August 20, 2014. Accepted August 23, 2014.
2010 Mathematics Subject Classification(s): Primary 81Q30; Secondary 32S40.
Key Words: Landau-Nakanishi geometry, hooked 3-lines graph, 3-particle threshold.
[*]Department of Mathematics, Faculty of Science, Hokkaido University, Sapporo, 060-0810, Japan.
Supported in part by JSPS KAKENHI Grant Number 23540178.
e-mail: honda@math.sci.hokudai.ac.jp
[**]Research Institute for Mathematical Sciences, Kyoto University, Kyoto, 606-8502, Japan.
Supported in part by JSPS KAKENHI Grant Number 24340026.
[***]Lawrence Berkeley National Laboratory, University of California, Berkeley, CA 94720, U.S.A.

Throughout this paper we use the same notations and terminologies used in [4] except for the wording "Landau-Nakanishi surfaces" (instead of "Landau-Nakanishi varieties") that means the projection of the Landau-Nakanishi varieties to the base manifold; for the sake of reference we also note that the notations and terminologies used here are basically the same as in [11]. In what follows "Landau-Nakanishi surfaces" are abbreviated to "LN surfaces".

Our conclusion is that the geometry is surprisingly simple and reasonable; we find a concretely defined exceptional set N, which we believe to correspond to what Sato ([11]) had in mind, at least near $3PT$, and we confirm (Section 3) that, outside a neighborhood of N, we encounter only finitely many positive-α LN surfaces associated with hooked 3-lines diagrams. Furthermore the singularities of the resulting surfaces are quite natural despite the appearance of higher codimensional components basically due to the existence of non-external vertices in hooked 3-lines diagrams. The higher codimensional components we encounter are simply intersections of real hypersurfaces (Sections 3 and 4), and we do not encounter any annoying singularities such as *acnodes*. As we note in Section 4, the existence of an acnode indicates the existence of (possibly infinitely many) complex singularities which accumulate to the acnode. The absence of acnodes in positive-α LN surfaces is consistent with the *strong asymptotic causality* (SAC) proposed in [1]. In Appendix A we further clarify the mechanism how acnodes appear in the study of LN surfaces in the real domain. We want to emphasize that the visualization of the LN surfaces with the help of a computer was an important step of our study to understand the origin of acnodes in LN surfaces ([3]). To stand on the safer side we note that we use the wording "*pinch (point)*" following the tradition in geometry; thus it is different from "pinch" used, say, in [3]. Our "pinch point" means the most singular point in *Whitney's umbrella*. (Cf. Appendix A.)

§ 2. Some preparations

As the first step toward a better understanding of the geometric aspect of Sato's postulates near the 3 particle threshold (= $3PT$) we study the positive-α Landau-Nakanishi surface $L^+(h_q)$ of a hooked 3-lines h_q defined below, having in mind the perturbation series expansion of the 3 to 3 S-matrix element. As noted in the introduction, we use the wording LN surfaces to mean the projection to the base manifold of the LN varieties in the cotangent bundle. We note that, in some context of our discussions below, we will be concerned with some particular higher codimensional components which are contained in the "surfaces".

In what follows we always assume that the space-time dimension is 2 and that the masses associated to the internal lines of the graph h_q are all equal to $m > 0$. We assume the graph h_q is oriented so that

(2.1) $\qquad k_{\ell,0} > 0$ holds for every internal line k_ℓ of h_q.

Definition 2.1. (i) A hooked 3-lines h_q with q hooks consists of 3 lines, the upper line, the middle line and the lower line, such that the middle line moves in a zigzag between the upper line and the lower line forming q hooks labeled by u (a hook formed by the upper line and the middle line) or d (a hook formed by the lower line and middle line) as shown below as an example in Figure 2.1.

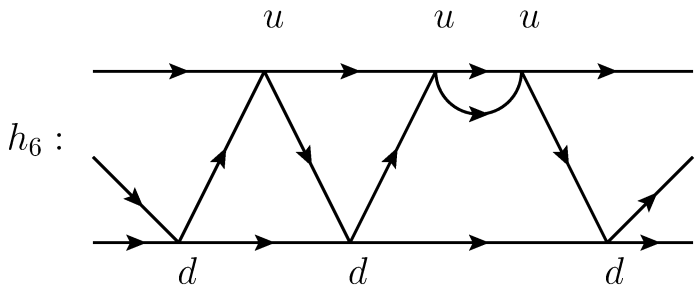

Figure 2.1. An example of a hooked 3-lines.

We identify, for example, h_6 in Figure 2.1 with the sequence of labels

(2.2) $\qquad duduud$ or $dudu^2d$ for short.

As a convention we assume that no u^p $(p \geq 3)$ or d^q $(q \geq 3)$ appears in the label.
(ii) If 3 lines meet at one point we label the point ϖ and call it a *pit*. A hooked 3-lines with a pit is called a pitted hooked 3-lines.

Remark 2.2. (i) As we are interested in the geometric aspect of the problem we have introduced the above convention; the positive-α LN surface associated with D_1 in Figure 2.2 coincides with that associated with D_2 in the same figure.

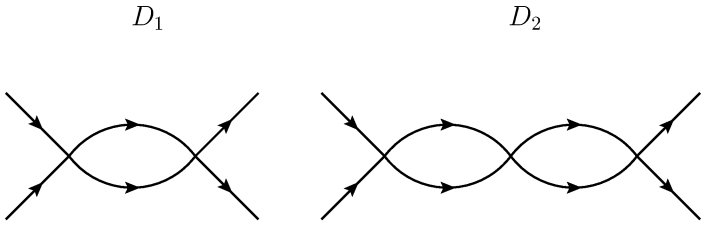

Figure 2.2.

(ii) A pitted hooked 3-lines graph is important in studying the contraction of a hooked 3-lines diagram; for example let us contract the leftmost slant in Figure 2.3 below.

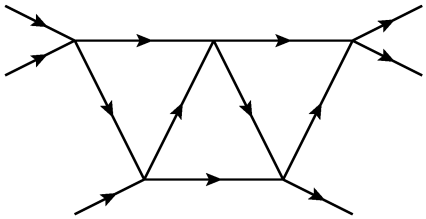

Figure 2.3.

Then we encounter the following pitted 3-lines in Figure 2.4.

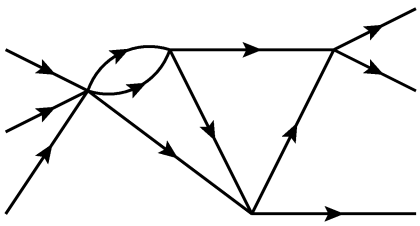

Figure 2.4.

In order to avoid possible confusions we always qualify a hooked 3-lines as pitted when it contains a pit.

(iii) In what follows, a *bead* means a part of the graph that has the form u^2 or d^2, using this wording, we find that a hooked 3-lines without beans is nothing but a *truss-bridge*

graph discussed in [4]. For example, the graph given in Figure 2.3 is a truss-bridge graph with 3 trusses, i.e., T_3 in the expressions of [4].

Definition 2.3. (i) We denote by $H(q)$ the totality of hooked 3-lines with q hooks.
(ii) We denote by ${}^{\varpi}H(q)$ (resp. $H^{\varpi}(q)$) the totality of a pitted hooked 3-lines whose leftmost (resp. rightmost) hook is a pit and which contains q hooks (including a pit).

Remark 2.4. For example, the graph given in Figure 2.4 belongs to ${}^{\varpi}H(4)$.

We next introduce the set N, which plays a central role in studying the geometric aspect of Sato's postulates.

Definition 2.5. The set N is, by definition, $N_+ \cup N_-$, where $N_\pm$ are given by the following:

$$N_+ = \bigcup_{k^2=m^2} \left\{ (p_1,p_2,p_3) \in \mathbb{R}^6; \begin{array}{l} p_{\sigma(1)} = k \text{ and } p_{\sigma(2)} + p_{\sigma(3)} = 2k \text{ hold} \\ \text{for some permutation } \sigma \text{ of } \{1,2,3\} \end{array} \right\}, \tag{2.3}$$

$$N_- = \bigcup_{k^2=m^2} \left\{ (p_4,p_5,p_6) \in \mathbb{R}^6; \begin{array}{l} p_{\tau(4)} = k \text{ and } p_{\tau(5)} + p_{\tau(6)} = 2k \text{ hold} \\ \text{for some permutation } \tau \text{ of } \{4,5,6\} \end{array} \right\}. \tag{2.4}$$

Remark 2.6. We often regard $N_\pm$ as subsets in $\mathbb{R}^{10} = \{(p_1,\dots,p_6) \in \mathbb{R}^{12};\ p_1 + p_2 + p_3 = p_4 + p_5 + p_6\}$.

Remark 2.7. We emphasize that $p_{\sigma(1)}$ and $p_{\tau(4)}$ are confined to be on mass-shell. As we will see in Section 3, this phenomenon is closely tied up with the existence of non-external vertices in the graph, i.e., the fact that the graph contains vertices upon which no external vectors are incident.

§ 3. Finiteness theorem for the leading positive-α Landau-Nakanishi surfaces outside N

Let us denote by $L^{\oplus}(G)$ the leading positive-α LN surface determined by the graph G, that is, the part of $L^{+}(G)$ where all $\alpha_\ell \gneqq 0$. Our first theorem is:

Theorem 3.1. *$L^{\oplus}(T_n) \subset N$ for $n \geq 4$.*

We note that we are considering the problem under the assumption that the space-time dimension is 2. Hence the following lemma is evident.

Lemma 3.2. *Suppose*

$$k_\ell^2 = m^2, \quad k_{\ell,0} > 0 \quad (\ell = 1, 2, 3, 4) \tag{3.1}$$

and

$$k_1 + k_2 = k_3 + k_4. \tag{3.2}$$

Then we find either

$$(k_3,\, k_4) = (k_1,\, k_2) \tag{3.3}$$

or

$$(k_3,\, k_4) = (k_2,\, k_1). \tag{3.4}$$

Proof of Theorem 3.1. To prove Theorem 3.1 using Lemma 3.2, we first consider the case $n = 4$. As will become clear later, the point is that T_4 contains two non-external vertices V and W below.

By applying Lemma 3.2 to the vertex V we find either [I] or [II] in Figure 3.1. Note that we abbreviate k_ℓ as ℓ in the subsequent figures.

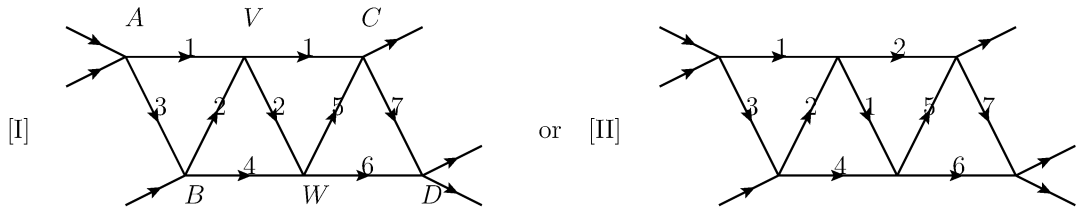

Figure 3.1.

Let us first consider the case [I]. Then it follows from the closed loop condition for the truss formed by B, V and W that

$$k_4 = k_2. \tag{3.5}$$

Hence Lemma 3.2 applied to the vertex W implies

$$k_5 = k_6 = k_2. \tag{3.6}$$

Hence the closed loop condition for the trusses $\triangle VWC$ and $\triangle CWD$ respectively entails

$$k_1 = k_2, \text{ and } k_7 = k_2. \tag{3.7}$$

Finally the closed loop condition for the leftmost truss $\triangle ABV$ reads as

$$k_3 = k_2, \tag{3.8}$$

as $k_1 = k_2$. Thus all k_ℓ's are the same, and hence we find

$$L^{\oplus}(T_4) \subset N \tag{3.9}$$

in case [I].

In case [II] we apply Lemma 3.2 to vertex W and separate the situation into 2 subcases [II.i] and [II.ii] in Figure 3.2 and Figure 3.3 respectively;

[II. i]

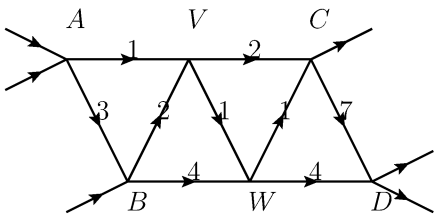

i.e. $(k_5, k_6) = (k_1, k_4)$,

Figure 3.2.

[II. ii]

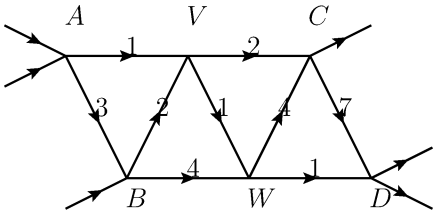

i.e. $(k_5, k_6) = (k_4, k_1)$.

Figure 3.3.

Let us first consider the case [II.i]. First, the closed loop condition for the truss $\triangle VWC$ implies

$$k_2 = k_1. \tag{3.10}$$

Then the closed loop condition for the truss $\triangle BVW$ entails

$$k_4 = k_1. \tag{3.11}$$

Hence the closed loop condition for the truss $\triangle WCD$ leads to

$$k_7 = k_1. \tag{3.12}$$

Similarly it follows from (3.10) that

$$k_3 = k_1. \tag{3.13}$$

Thus we find all the internal lines are equal in [II.i]. The reasoning in the situation [II.ii] is slightly subtler; we consider two trusses $\triangle BVW$ and $\triangle VWC$ simultaneously to deduce from the closed loop conditions for them that

$$k_2 = k_4. \tag{3.14}$$

Hence the closed loop condition for the truss $\triangle BVW$ implies

$$k_1 = k_2, \tag{3.15}$$

showing also

$$k_3 = k_7 = k_2. \tag{3.16}$$

Thus we have confirmed

$$L^{\oplus}(T_4) \subset N; \tag{3.17}$$

we note that in our reasoning we have used only the fact that both V and W are non-external vertices, together with the closed loop conditions for several trusses. Thus it is clear that all the internal vectors that appear in the configuration of $L^{\oplus}(T_n)$ $(n \geq 5)$ are the same, and hence we find

$$L^{\oplus}(T_n) \subset N. \tag{3.18}$$

This completes the proof of Theorem 3.1. □

Remark 3.3. An important point in Theorem 3.1 is that, although the external vector p_r $(r = 1, 2, \ldots, 6)$ are not confined to the mass-shell manifold in the Landau-Nakanishi equations, which we are using in this paper, some external vectors are confined to the mass-shell manifold in the leading positive-α LN surfaces $L^{\oplus}(T_n)$ $(n \geq 4)$.

In parallel with Theorem 3.1 we find the following.

Theorem 3.4. *If the number q of the hooks is equal to or bigger than* 12*, then*

$$L^{\oplus}(h_q) \subset N \tag{3.19}$$

holds.

Proof. Let (p, k) be the set of vectors which realizes the diagram $L^{\oplus}(h_q)$, and let $\{k_\ell\}_{\ell \in R}$ be the totality of internal vectors that do not form a bead in h_q. Then, by the procedure to be described below, we use $(p, \{k_\ell\}_{\ell \in R})$ to form a configuration $L^{\oplus}(T_n)$, where T_n is a truss-bridge graph with $\tilde{q}$ vertices, where $\tilde{q} \geq q/2$.

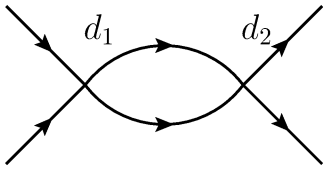

Figure 3.4.

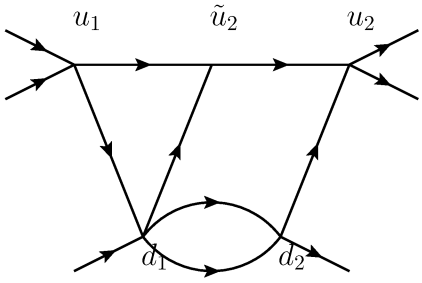

Figure 3.5.

The procedure is as follows: first, we note that, for some bead (see Figure 3.4) which is with some internal lines being incident upon each of vertices d_1 and d_2, we find a part $u_1 d_1 d_2 u_2$ in h_q because of the convention that d^3 is not allows in h_q. Then we can form a triangle using the vectors associated with $u_1 d_1$ and $u_1 d_1$ together with the parallel displacement of the vector associated with $d_2 u_2$ so that it may leave from d_1 as indicated in Figure 3.5 where $d_1 \tilde{u}_2$ is parallel to $d_2 u_2$. On the other hand, if two lines entering d_1 or two lines leaving from d_2 are external, then we just collapse the bead $d_1 d_2$.

By this procedure we find a leading positive-α Landau-Nakanishi surface $L^{\oplus}(T_n)$ associated with a truss-bridge graph T_n with $\tilde{q}$ vertices, where

$$\tilde{q} = q - \#(\text{beads in } h_q)/2 \geq q/2.$$

Since q is supposed to be bigger than or equal to 12, the number of trusses in T_n, i.e., n is bigger than or equal to 4. Hence Theorem 3.1 entails the point p in question is in N. □

Remark 3.5. Although the number 4 in Theorem 3.1 is the best possible one, the number 12 in Theorem 3.4 is not so. For example we can easily confirm

$$L^{\oplus}(u^2 d u d^2) \subset N. \tag{3.20}$$

But, at the same time, one can confirm that $L^{\oplus}(u^2 d u^2 d)$ is not contained in N, as we find the following configuration described in Figure 3.6 by making use of the so-called *ice-cream cone diagram* in Figure 3.7. (See Section 5 [II] for the details.) By examining

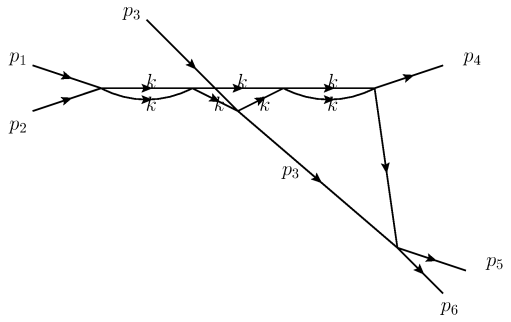

Figure 3.6.

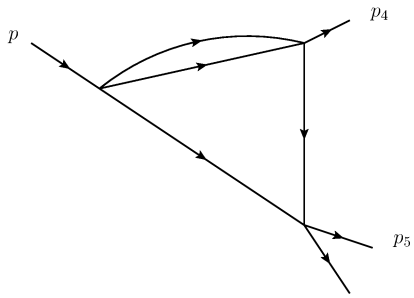

Figure 3.7.

all the cases individually we can find that the best possible number q in Theorem 3.4 is 8; we find

$$L^{\oplus}(h_q) \subset N \quad \text{if } q \geq 8. \tag{3.21}$$

We leave the concrete verification of (3.21) to the reader, but as a typical example we show how to confirm

$$L^{\oplus}(u^2d^2u^2d^2) \subset N. \tag{3.22}$$

It is clear that the truss-bridge graph used in the proof of Theorem 3.4 is T_2. However, by keeping the beads in the diagram in Figure 3.8 below, we confirm (3.22) as follows: in Figure 3.8 Lemma 3.2 implies $DE = DG = k$ and $BE = DE = \ell$. Hence $\ell = k$.

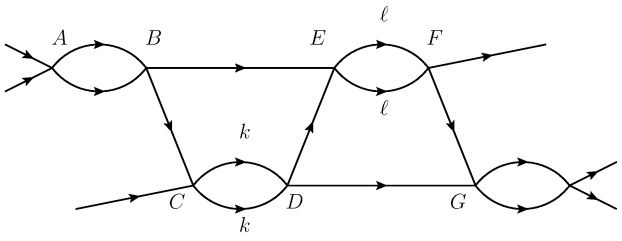

Figure 3.8.

Then the closed loop conditions entail $BC = FG = k$. Again by using Lemma 3.2 we then find all internal lines in $L^{\oplus}(u^2d^2u^2d^2)$ are equal to k. By the reasoning of this sort we can confirm

$$L^{\oplus}(h) \subset N \quad \text{for any } h \text{ in } H(8) \tag{3.23}$$

by checking all hooked 3-lines with 8 hooks individually. On the other hand, it follows from the definition of a hooked 3-lines diagram that, if

$$L^{\oplus}(h) \subset N \quad \text{holds for every } h \text{ in } H(q), \tag{3.24}$$

then

$$L^{\oplus}(\tilde{h}) \subset N \quad \text{holds for any } \tilde{h} \text{ in } H(q+1). \tag{3.25}$$

Thus we can prove Theorem 3.4 by the induction on q, starting from $q = 8$.

Remark 3.6. In the course of the study mentioned in the preceding remark, we have obtained the following list of hooked 3-lines whose leftmost hook is u and that gives us leading positive-α LN surfaces that are not contained in N. We have listed only one graph among graphs which are topologically isomorphic, like D_1 and D_2 in Figure 3.9.

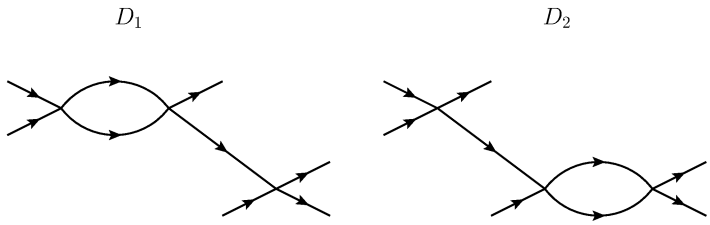

Figure 3.9.

[I] $H(1)$: The diagram in Figure 3.10.

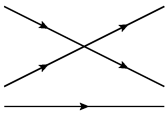

Figure 3.10. $H(1)$.

[II] $H(2)$: The ones in Figures 3.11 and 3.12.
[III] $H(3)$: The ones in Figures 3.13 and 3.14.
[IV] $H(4)$: The ones in Figures 3.15, 3.16, 3.17 and 3.18.
[V] $H(5)$: The ones in Figures 3.19, 3.20, 3.21, 3.22 and 3.23.
[VI] $H(6)$: The ones in Figures 3.24 and 3.25.
[VII] $H(7)$: The one in Figure 3.26.

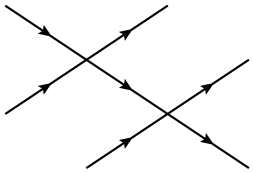

Figure 3.11. $H(2)$.

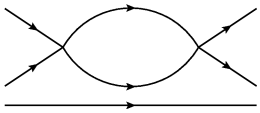

Figure 3.12. $H(2)$.

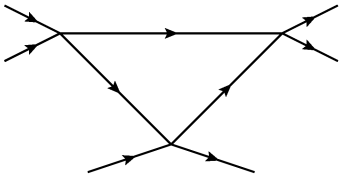

Figure 3.13. $H(3)$.

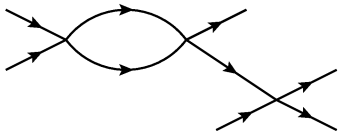

Figure 3.14. $H(3)$.

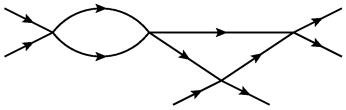

Figure 3.15. H(4).

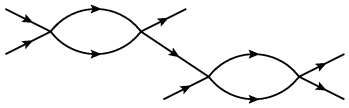

Figure 3.16. $H(4)$.

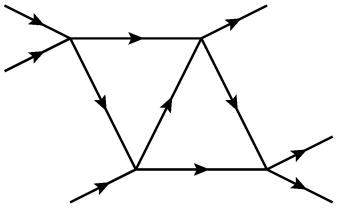

Figure 3.17. $H(4)$ T_2.

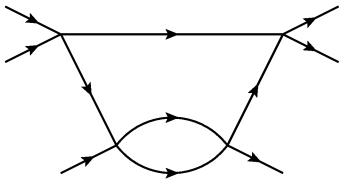

Figure 3.18. $H(4)$.

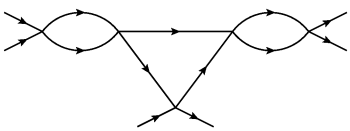

Figure 3.19. $H(5)$.

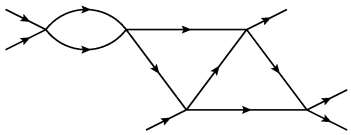

Figure 3.20. $H(5)$.

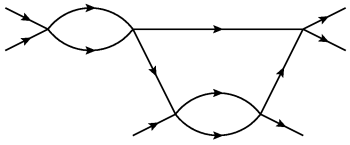

Figure 3.21. $H(5)$.

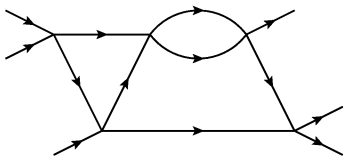

Figure 3.22. $H(5)$.

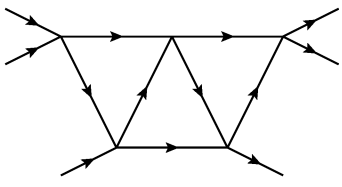

Figure 3.23. $H(5)$ T_3.

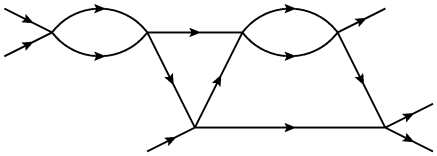

Figure 3.24. $H(6)$.

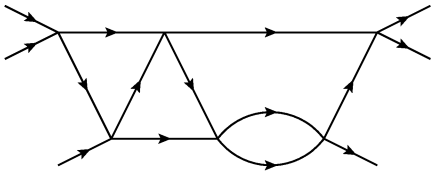

Figure 3.25. $H(6)$.

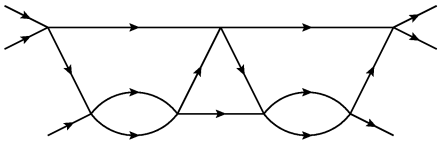

Figure 3.26. $H(7)$.

Remark 3.7. The leading positive-α LN surfaces associated with Figures 3.15 and 3.19 might be regarded to be contained in N, because all the internal lines are parallel, but we keep them in this list in view of our definition of N, which is given in terms of the conditions on external lines.

Remark 3.8. The diagram in Figure 3.24 is the same as that of Figure 3.6 in Remark 3.5. The leading positive-α LN surfaces for diagrams in Figures 3.20, 3.22, 3.25 and 3.26 can be found also with the help of the ice-cream cone diagram in Figure 3.7.

Remark 3.9. All diagrams listed in Remark 3.6 play important roles in our subsequent reasoning. Although some of them (e.g., those mentioned in Remark 3.8) are of higher codimension, they are all intersections of real hypersurfaces, as we will see later. We also note that, with the understanding in Remark 3.7, we first find in $H(6)$ a hooked 3-lines diagram whose leading positive-α LN surface is contained in N, like Figures 3.27, 3.28, 3.29 and so on.

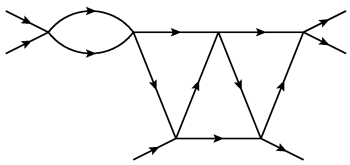

Figure 3.27.

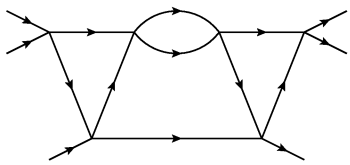

Figure 3.28.

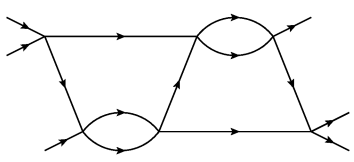

Figure 3.29.

Needless to say, T_4 is among them, as we have seen in Theorem 3.1.

In Section 4 we further need the following.

Theorem 3.10. *For h in ${}^{\varpi}H(q)$ $(q \geq 4)$ we find*

$$L^{\oplus}(h) \subset N. \tag{3.26}$$

Proof. In view of the definition of ${}^{\varpi}H(q)$, we find that it suffices to confirm (3.26)

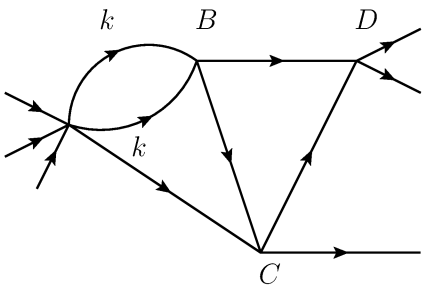

Figure 3.30.

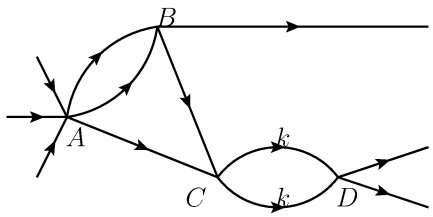

Figure 3.31.

for h in ${}^{\varpi}H(4)$. Clearly we may assume without loss of generality that the leftmost two hooks of h is ϖu. Since ϖ may be regarded as either u or d arbitrarily, ϖu^2 is not allowed by our convention. Hence h has the form ϖudu or ϖud^2; the leading positive-α LN surface of ϖudu is described as $L^{\oplus}$("the diagram in Figure 3.30").

Then Lemma 3.2 implies that $BC = BD = k$, and hence by the closed loop conditions we find that all the internal vectors are equal to k. Thus we find (3.26) for $h = \varpi udu$. For the leading positive-α LN surface of $h = \varpi ud^2$, the configuration is given by $L^{\oplus}$("the diagram in Figure 3.31"). Again by Lemma 3.2 we find that $AC = BC = k$, and hence by the closed loop condition we find that all internal vectors are equal to k. Thus we have confirmed (3.26) for h in ${}^{\varpi}H(4)$, completing the proof of Theorem 3.10. □

§ 4. Landau-Nakanishi surfaces near the 3 particle threshold (= $3PT$)

The result in Section 3 give the impression that the exceptional set that [11] mentions is the set N near $3PT$. However, a wider region might be needed in the context of [11] p. 25, because we have so far discussed positive-α LN surfaces; as [3] p. 106 indicates, a positive-α LN surface, as an object in the real domain by its definition, might contain singularities originating from complexified LN surfaces. For example, if there were two real-valued real analytic function $f(p)$ and $g(p)$ such that there exists a real point p_0 in $3PT$, but outside N, where

$$f(p_0) = g(p_0) = 0, \tag{4.1}$$

and

$$\text{grad}_p\, f(p) \text{ and } \text{grad}_p\, g(p) \text{ are linearly independent at } p_0, \tag{4.2}$$

and if the complexification of the positive-α LN surface had components L_n ($n = 1, 2, 3, \dots$) given by

$$(f(p) + \sqrt{-1}ng(p))(f(p) - \sqrt{-1}ng(p)) = 0, \tag{4.3}$$

then such a point p_0 should be included in the exceptional set in the sense of [11] p. 25. Although non-existence of such points in the leading positive-α LN surfaces follow from the strong asymptotic causality condition ([1], [7]) we want to confirm this directly and, more important, in a domain "slightly" outside physical region. For this purpose we want to study concretely $\cup_h L^+(h)$ near $3PT$, but outside N, where h ranges over $\cup_q H(q)$. The subtlety of the notion of the complexification in this context is explained in Appendix A.

Thus our first task is to list up all positive-α LN surfaces associated with hooked 3-lines diagrams that may have some intersections with $3PT$ outside N. We will then study their geometric characters in detail in Section 5. Here we note that it is not in general enough to employ the complex Landau-Nakanishi equations to describe the characteristic variety of the holonomic system that the Feynman function in question satisfies. To be more precise, Landau-Nakanishi equations are not adequate to describe the cotangential component of the characteristic variety in consideration except for rather restricted cases. (Cf. [9], [11].) Hence in this paper and the subsequent one ([6]) we first consider positive-α LN surfaces and their local complexification, and we then try to dominate the characteristic variety by the union of the closure of the conormal set of each stratum of the stratification of the locally complexified LN surfaces. The discussion in what follows is designed to be the first step toward this program.

To begin with we show the following.

Proposition 4.1. *Positive-α LN surfaces associated with $\cup_q {}^{\varpi}H(q)$ that may intersect with $3PT$ outside N are given by some of the following diagrams $(a) \sim (e)$ below if we list up only one among isomorphic ones such as diagrams in Figures 4.1 and 4.2.*

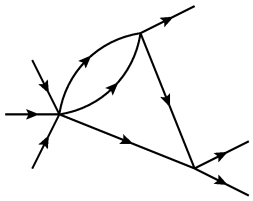

Figure 4.1.

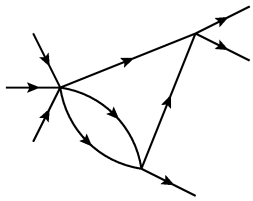

Figure 4.2.

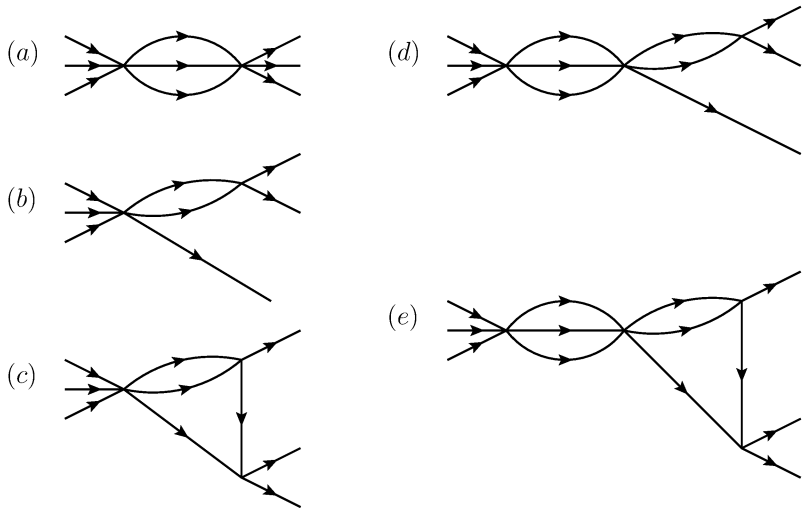

Figure 4.3.

Proof. As ${}^{\varpi}H(1)$ contains only the diagram in Figure 4.4, we study elements in

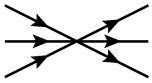

Figure 4.4.

${}^{\varpi}H(q)$ with $q \geq 2$. We choose ϖu in ${}^{\varpi}H(2)$, which is isomorphic to another element ϖd

in ${}^{\varpi}H(2)$. The positive-α LN surface associated with ϖu is a two particle threshold given by (b), and it is not our main concern. But it still intersect with $3PT$, and it plays an important role in making our subsequent induction run smoothly. As a representative element of ${}^{\varpi}H(3)$, we can choose without loss of generality the so-called

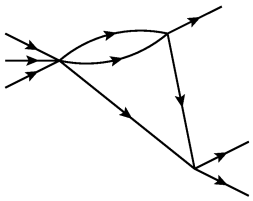

Figure 4.5.

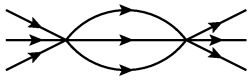

Figure 4.6.

ice-cream cone diagram in Figure 4.5, whose positive-α LN surface (i.e., the union of LN surfaces associated with some contraction of the ice-cream cone diagram) contains the diagram in Figure 4.6. For h in ${}^{\varpi}H(4)$ we know by Theorem 3.10 that

$$L^{\oplus}(h) \subset N, \tag{4.4}$$

and hence we have to contract some internal lines of h to find positive-α LN surfaces which are not contained in N. We may assume without loss of generality that h in ${}^{\varpi}H(4)$ to be studied has the form in Figure 4.7 or Figure 4.8.

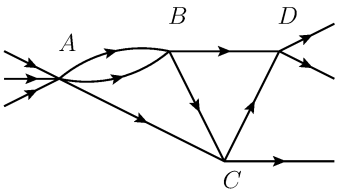

Figure 4.7.

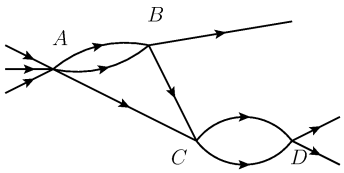

Figure 4.8.

Let us first consider the case in Figure 4.7. Then we can readily confirm that the contractions of the diagram in Figure 4.7 result in

- the diagram in Figure 4.9 through the contraction of AB,
- the one in Figure 4.10 through the contraction of BC,
- the one in Figure 4.11 through the contraction of AC,
- the one in Figure 4.12 through the contraction of BD,

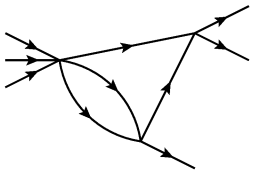

Figure 4.9.

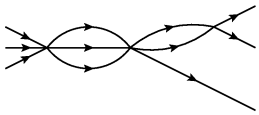

Figure 4.10.

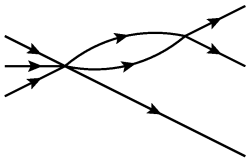

Figure 4.11.

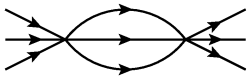

Figure 4.12.

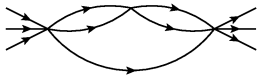

Figure 4.13.

- or the one in Figure 4.13 through the contraction of CD.

Here we note that the contraction of AC (resp. BD) forces the contraction of $\triangle ABC$ (resp. $\triangle BCD$) because of the orientation of relevant segments. We also note that we regard both-ends-pitted elements such as Figure 4.13 to be equivalent to Figure 4.12, as we are concerned with the geometric aspect of the problem.

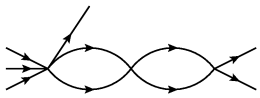

Figure 4.14.

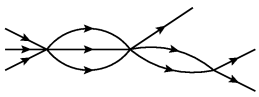

Figure 4.15.

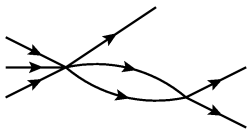

Figure 4.16.

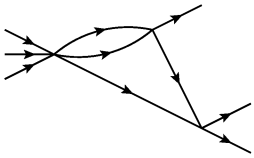

Figure 4.17.

Next we consider the case in Figure 4.8. Then we find that its contractions result in

- the diagram in Figure 4.14 through the contraction of AB,
- the one in Figure 4.15 through the contraction of BC,
- the one in Figure 4.16 through the contraction of AC (and hence that of $\triangle ABC$),
- or the one in Figure 4.17 through the contraction of CD.

Thus we have found $(a) \sim (d)$; the remaining one (e) found by examining h is in ${}^{\varpi}H(5)$.

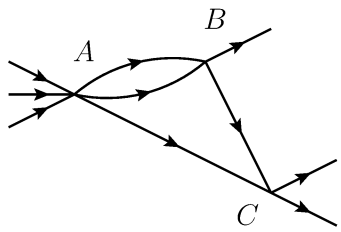

Figure 4.18.

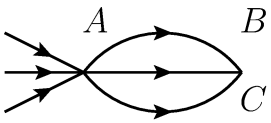

Figure 4.19.

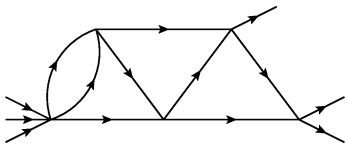

Figure 4.20.

We may assume the left-most 3 hooks of h to be studied has the form in Figure 4.18. Then by contracting AB, we find an element in ${}^{\varpi}H(4)$, whereas the contraction of BC results in a diagram in which Figure 4.19 is hinged at its right-end with another element g in ${}^{\varpi}H(3)$; actually if the starting h in ${}^{\varpi}H(5)$ is the diagram in Figure 4.20, the diagram g is the ice-cream cone diagram. Thus we find (e).

By examining other elements in ${}^{\varpi}H(5)$ whose left-most 3 hooks are ϖud, namely, ϖudu^2 and ϖud^2u, we find the diagrams $(a) \sim (e)$ cover all the cases.

For h in ${}^{\varpi}H(q)$ $(q \geq 6)$, we know

$$L^{\oplus}(h) \subset N, \tag{4.5}$$

and hence we should contract some internal lines of h to find a positive-α LN surface outside N. If the contraction is made in the ice-cream cone diagram located in the left-most part of h, the same reasoning as that used for Figure 4.20 yields some $\tilde{h}$ in ${}^{\varpi}H(q')$ $(q' \leq q-1)$ or the diagram in Figure 4.21 hinged with some g in ${}^{\varpi}H(q-2)$

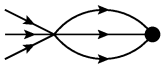

Figure 4.21.

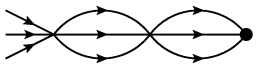

Figure 4.22.

from the right since we regard the diagram in Figure 4.22 to be the same as the one in Figure 4.21 in this paper, the resulting diagram is given by one of $(a) \sim (e)$. If the contraction is made in other parts, we find a both-ends-pitted diagram hinged with $\tilde{g}$ in ${}^{\varpi}H(q')$ $(q' \leq q-2)$ from right; since the both-sides-pitted part is regarded to be equivalent to Figure 4.21, the resulting diagram is again given by one of $(a) \sim (e)$. This completes the proof of the proposition. □

Completely in parallel with Proposition 4.1 we find

Proposition 4.2. *Positive-α LN surfaces associated with $\cup_q H^{\varpi}(q)$ that may intersect with $3PT$ outside N are given by some of the following diagrams $(a') \sim (e')$*

given below, if we list only one among isomorphic ones such as Figure 4.23 and Figure 4.24.

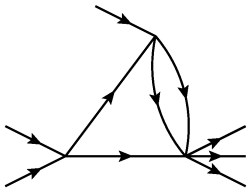

Figure 4.23.

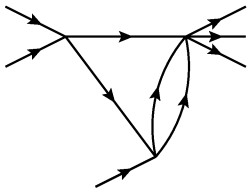

Figure 4.24.

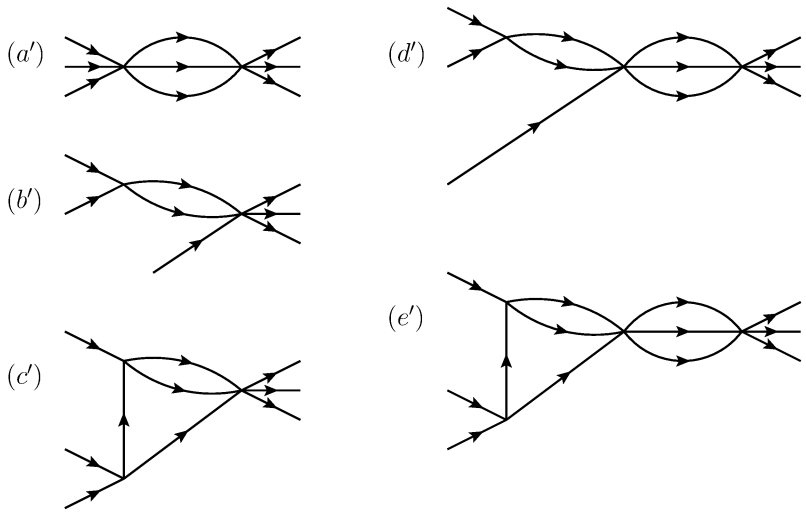

Figure 4.25.

To summarize our results in Theorem 4.6 below we prepare the following definitions.

Definition 4.3. If a hooked 3-lines diagram h has the form

$$g \cdot g' \tag{4.6}$$

where g (resp. g') is in $H^{\varpi}(q)$ (resp. ${}^{\varpi}H(q')$) and $g \cdot g'$ means they are hinged at the rightmost (resp. leftmost) pit of g (resp. g'), then we say h is a *pinned* 3*-lines diagram*, and the totality of pinned 3-lines diagrams is denoted by $\wp$.

Remark 4.4. A typical example of a pinned 3-lines diagram is the one in Figure 4.26 which appears as the contraction of the middle slant u_2d_2 of T_4 given in Figure 4.27.

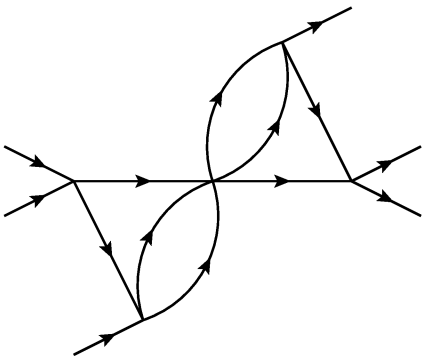

Figure 4.26.

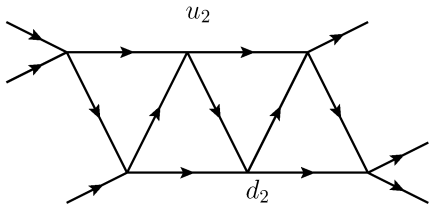

Figure 4.27.

Definition 4.5. Let L denote

$$\cup_{h\in\mathcal{B}} L^{+}(h), \tag{4.7}$$

where $\mathcal{B}$ denotes the following set:

$$\begin{aligned}&(\cup_{q\leq 5}H(q))\bigcup(\cup_{q\leq 3}({}^{\varpi}H(q)\cup H^{\varpi}(q)))\bigcup\\&\{h\in\wp \text{ with } h=g\cdot g', \text{ where } g\in\cup_{q\leq 3}H^{\varpi}(q) \text{ and } g'\in\cup_{q\leq 3}{}^{\varpi}H(q)\ \}.\end{aligned} \tag{4.8}$$

With these terminologies we find

Theorem 4.6. *For any h in $H(q)$ $(q\geq 6)$ its positive-α LN surface $L^{+}(h)$ is contained in L outside N.*

Proof. Let us first consider the case when h is in $H(6)$. Then we find the following two diagrams $h(1)$ in Figure 4.28 and $h(2)$ in Figure 4.29 are the elements in $H(6)$ whose leading positive-α LN surfaces are not contained in N. (Cf. Remark 3.6 [VI].) As is noted in Remark 3.8, their leading positive-α LN surfaces are realized respectively as configurations in Figures 4.30 and Figures 4.31.

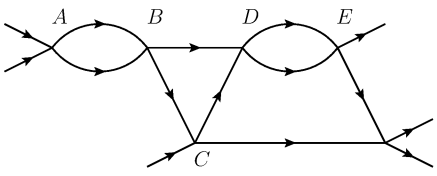

Figure 4.28. $h(1)$.

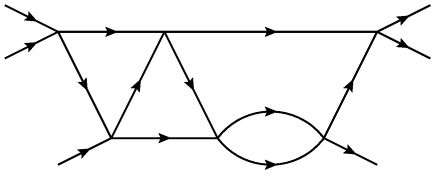

Figure 4.29. $h(2)$.

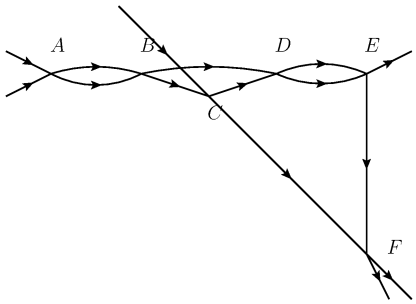

Figure 4.30.

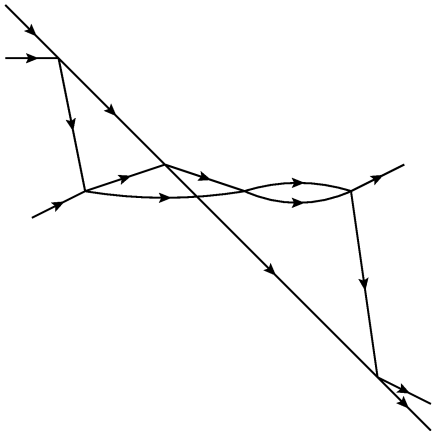

Figure 4.31.

Let us first consider the case in Figure 4.30. In this case AB, BC, CD and DE are all parallel. Hence, by keeping all vectors (p, k) intact, we can slide the vertices B and D so that either of them may coincide with C; thus we find

$$L^{\oplus}(h(1)) \subset L^{\oplus}(h(3)) \cap L^{\oplus}(h(4)), \tag{4.9}$$

where $h(3)$ and $h(4)$ are in Figures 4.32 and 4.33 respectively.

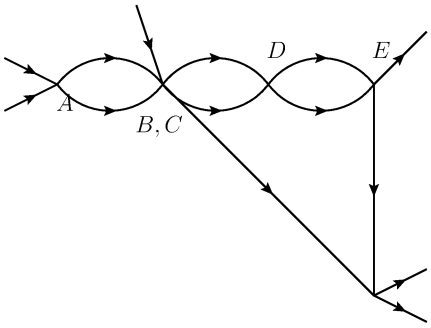

Figure 4.32. $h(3)$.

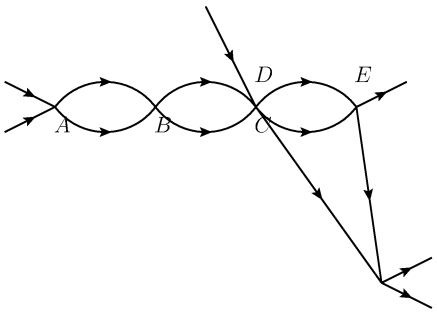

Figure 4.33. $h(4)$.

Since we are concerned only with the location of singularities, ignoring the problem related to the multiplicity, we find $L^{\oplus}(h(3))$ and $L^{\oplus}(h(4))$ coincide; they are described by the pinned diagram $(b') \cdot (c)$. If we want to consider the positive-α LN surface determined by some contraction of $h(1)$, it is almost evident that it should be handled by some hooked 3-lines, possibly pitted or pinned, with q hooks with $q \leq 5$. To stand on the safer side, let us described the procedure concretely. We hope the argument below may help the reader to understand logical structure of our reasoning.

If the contraction is performed at a bead, then the resulting diagram belongs to $H(5)$. Hence its positive-α LN surface is contained in L. If we contract a slant (i.e., ud or du) a pit appears and hence the contracted diagram either belongs to $H^{\varpi}(5)$ or has the pinned form

$$g \cdot g' \tag{4.10}$$

where g (resp. g') is in $H^{\varpi}(\ell)$ (resp. ${}^{\varpi}H(r)$) with $\ell + r \leq 6$ ($\ell, r \geq 1$). (In general, it may belong to ${}^{\varpi}H(5)$, but in the case of $h(1)$ this cannot be observed. We encounter some element in ${}^{\varpi}H(5)$ in the same reasoning applied to $h(2)$.) Parenthetically we note that, because of the orientation of the diagram in question, contraction of internal lines which are neither slants nor beads forces some slant automatically contracted; for example if BD in $h(1)$ is contracted, then the triangle $\triangle BCD$ is contracted out.

Let us return to (4.10); if ℓ (resp. r) is equal to or bigger than 4, then we further contract internal lines of g (resp. g') to find a positive-α LN surface outside N. Thus we eventually find

$$\ell, r \leq 3 \tag{4.11}$$

in (4.10). Thus we have confirmed that the positive-α LN surface determined by $h(1)$ (including its contractions) is contained in L.

The above reasoning for $h(1)$ is equally applicable to $h(2)$; this time the counterpart of (4.9) is

$$L^{\oplus}(h(2)) \subset L^{\oplus}(h(5)), \tag{4.12}$$

where $h(5)$ denotes the hinged ice-cream cone diagrams given by Figure 4.26. Then the rest of the reasoning in dealing with the contracted diagrams is exactly the same as in the case of $h(1)$.

It is now clear how to argue for h in $H(6)$ which is different from $h(1)$ or $h(2)$. For such h we know

$$L^{\oplus}(h) \subset N \tag{4.13}$$

and hence we are to contract some of its internal lines. Then the argument is exactly the same as in handling the contracted diagrams of $h(1)$. Thus we have confirmed Theorem 4.6 for h in $H(6)$.

The above reasoning equally applies to $H(7)$; the only element in $H(7)$ whose leading positive-α LN surface is not contained in N is

$$h(6) = ud^2ud^2u, \tag{4.14}$$

and $L^{\oplus}(h(6))$ is realized by the following configuration in Figure 4.34 where AB, BC,

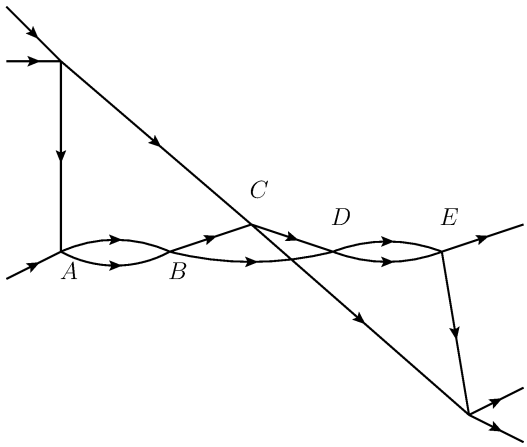

Figure 4.34.

BD, CD and DE are all parallel. As in the case of $h(1)$, we then find

$$L^{\oplus}(h(6)) \subset L^{\oplus}(h(5)); \tag{4.15}$$

thus the geometric result is the same for $h(2)$, and the reasoning for handling the contraction goes equally well as in the case of $h(1)$, since our understanding of LN surfaces for h in $H(6)$ has already been completed. It is clear that the treatment of other elements in $H(7)$ can be done in a similar manner.

Since

$$L^{\oplus}(h) \subset N \tag{4.16}$$

holds for any h in $H(q)$ $(q \geq 8)$, we can confirm by the induction on q that $L^{+}(h)$ is contained in L for any h in $H(q)$ $(q \geq 8)$. This completes the proof of Theorem 4.6. □

§ 5. Concrete description of Landau-Nakanishi surfaces of some basic diagrams in $\cup H(q)$

In view of Theorem 4.6 we now want to study the concrete shape of the positive-α LN surfaces associated with a (possibly pitted or pinned) hooked 3-lines diagrams in $\mathcal{B}$, so that we may confirm that they do not contain, at least near $3PT$, any pathological singularities such as acnodes; as we will show in Appendix A there are some delicate issues relevant to acnodes and cusps from the theoretical viewpoint. As this paper is designed to be the first step in the better understanding of [11], we content ourselves here in concretely describing the LN surfaces associated with some basic diagrams in $\mathcal{B}$ with the help of a computer. Here we note that we use a computer so that it may draw a figure using the exact formula. See Appendix A for example.

In our subsequent paper ([6]) we plan to make some more analytic (vs. geometric) study of this issue from the view point of holonomic structure of Feynman integrals in question.

[I] The first diagram we want to study is the ice-cream cone diagram I_R:

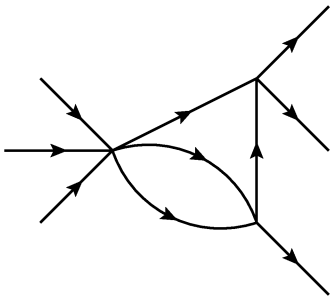

Figure 5.1.

The leading real (i.e., not necessarily positive-α) LN surface $L^{\times}(I_R)$ is described in [4] Figure 1. The surface presents the so-called Whitney's umbrella, as shown below in Figure 5.2. Here we observe a pinch point singularity at N_- and a cusp (self-intersection points) emanating from the pinch point. An important point is that, outside N_-, the cusp does not appear in the positive-α LN surface $L^{+}(I_R)$. Thus its "slice" outside N_- takes the form in Figure 5.3, where the dotted part designates the slice of non-positive-α part of $L^{\times}(I_R)$; the curved segment C_2C_3 shrinks as we let the slice approach to N_-, and eventually at N_- they coincide with N_-. Thus we do not observe any pathologies near C_3 outside N_-.

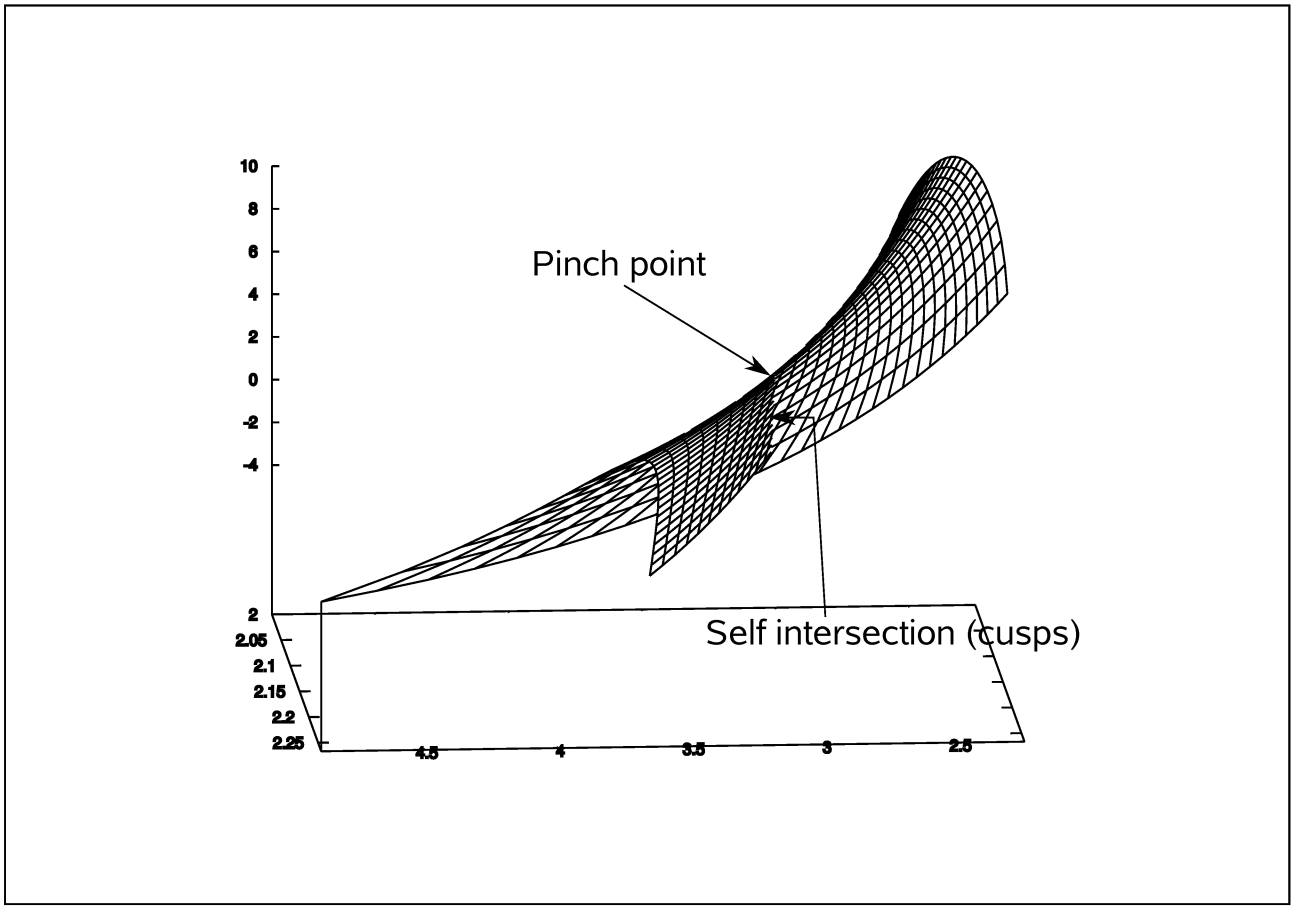

Figure 5.2. The shapes of $L^{\times}(I_R)$ and $L^{\oplus}(I_R)$ are the almost same as those of T_1. See Figures A.2 and A.3 in Appendix A also.

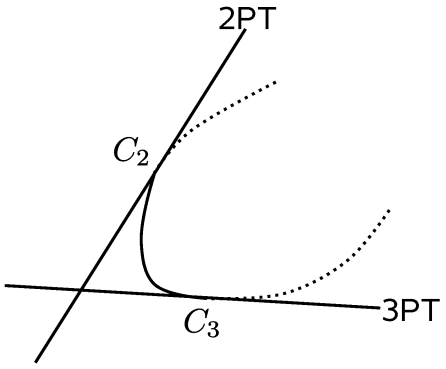

Figure 5.3.

[II] The second example we study is T_2, which is the same as the so-called crossed square diagram given by Figure 5.4.

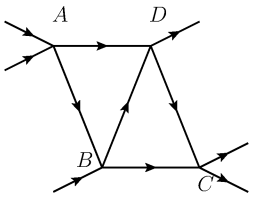

Figure 5.4.

Assuming that we consider its leading real LN surface outside N, it takes the form in Figure 5.5.

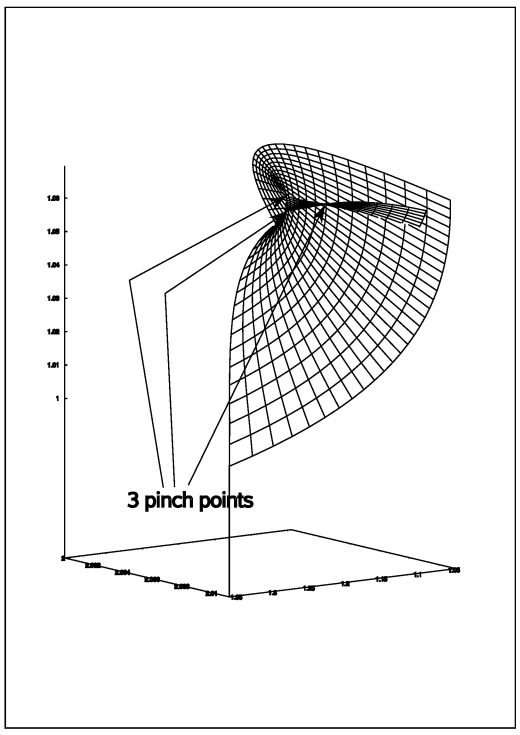

Figure 5.5. $L^{\times}(T_2)$ viewed in the far distance.

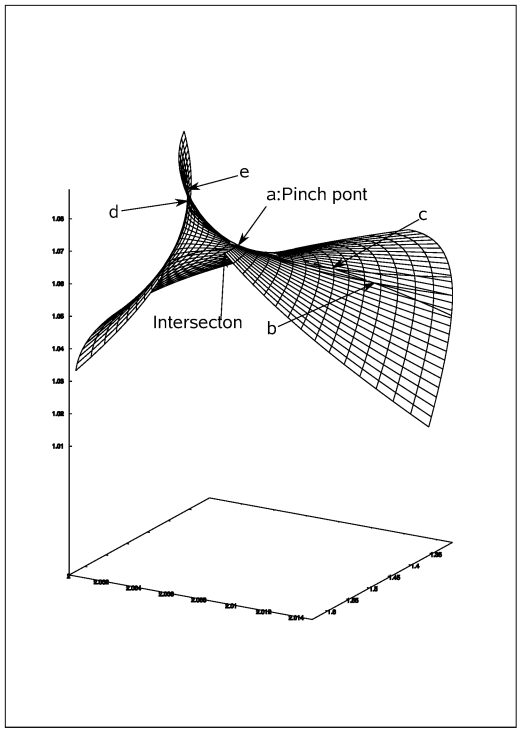

Figure 5.6. The positive-α parts of $L^{\times}(T_2)$ are $\triangle abc$ and $\triangle ade$ on the surface.

We observe 3 pinch points and several cusps passing through the pinch points. However, we can confirm that the cusps are not contained in the positive-α region. At the same time we also find that at least 2 pinch points P_1 and P_3 are associated with the positive-α Landau-Nakanishi diagram. (The pinch point P_2 is a limiting point of

a sequence of points in positive-α LN surface.) These 3 pinch points merge at N, but more important is the following fact; the pinch point P_1 is associated with the following diagram D_0 in Figure 5.7:

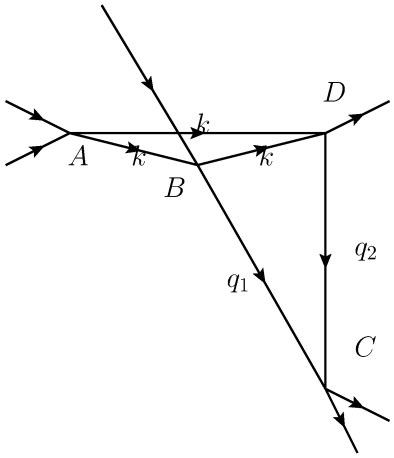

Figure 5.7. The diagram D_0.

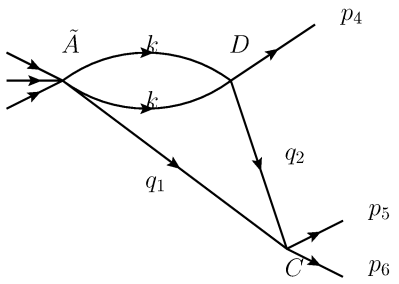

Figure 5.8.

In order to confirm that $L^{\oplus}(D_0)$ can be realized in the above form, we argue as follows: first we consider $L^{\oplus}$("the diagram in Figure 5.8") which has the form

$$\{p; \varphi(p_C, p_D) = 0, \text{ where } p_C = p_5 + p_6\}. \tag{5.1}$$

Then (q_1, q_2, k) is determined by p_c and p_D, as u-vectors in the LN equations are described in this case by $\mathrm{grad}_{(p_C, p_D)}\, \varphi$. Using (q_1, q_2, k), we realize the configuration D_0 in Figure 5.9 by choosing the triangle $\triangle BCD$ to be the same as $\triangle \tilde{A}CD$, $u_B - u_A = \alpha k$

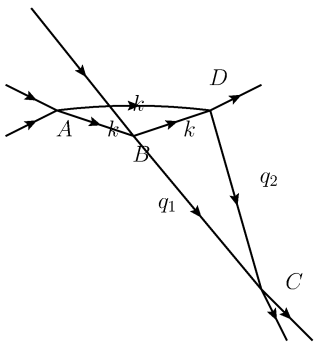

Figure 5.9. The configuration D_0.

for an arbitrary positive number α and $(p_A, p_B) = (2k, q_1)$. This construction of the

diagram D_0 shows

$$L^{\oplus}(D_0) \subset \{\varphi(p_C, p_D) = 0\} \cap \{p_A = 2k\}. \tag{5.2}$$

Thus we find

$$\operatorname{codim} L^{\oplus}(D_0) = 3. \tag{5.3}$$

Needless to say, we have

$$p_A^2 = 4m^2, \tag{5.4}$$

and hence

$$L^{\oplus}(D_0) \subset \{\varphi(p_C, p_D) = 0\} \cap \{p_A^2 = 4m^2\}. \tag{5.5}$$

In view of this geometry, we feel it worth noting its resemblance to, and at the same time, its difference from Figure 5.10. (Cf. Remark 3.8; this configuration appears, when we delete the leftmost bead in Figure 3.6 to simplify the logical structure of the discussion below.) In diagram D_1, we use the flexibility of the vertex F so that we may

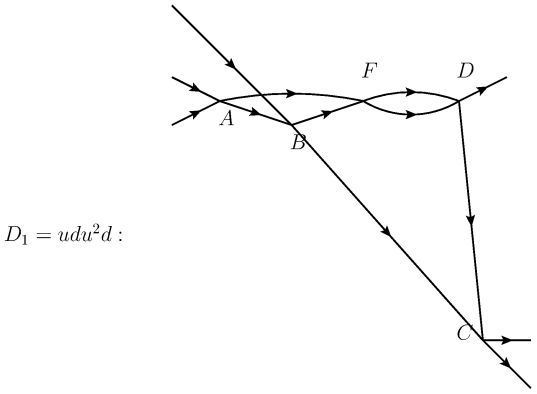

Figure 5.10. $D_1 = udu^2d$.

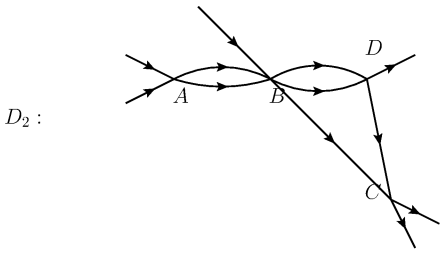

Figure 5.11. D_2.

reach the configuration D_2 in Figure 5.11 with keeping the external vectors (and hence the internal vectors also) intact. Although

$$L^{\oplus}(D_2) \subset \{\varphi(p_C, p_D) = 0\} \cap \{p_A^2 = 4m^2\}, \tag{5.6}$$

we cannot reach D_2 by changing the Landau constants α_ℓ's in D_0. This difference of D_0 and D_1 indicates the difference of holonomic structure of F_{T_2} and F_h ($h = udu^2d$). Actually, as we will see in [6], F_{T_2} satisfies a simple holonomic microdifferential equations, whereas the multiplicity of the holonomic system that F_h satisfies is bigger than 1.

As the principal purpose of this paper is to clarify the geometric situation of the intersection of $3PT$ and the positive-α LN surfaces associated with hooked 3-lines diagrams, and as the pinch point in question is away from $3PT$ outside N, we had better stop our discussion around here concerning the problems relevant to the pinch points. But we cannot resist the temptation to raise, at least, the following question: through the contraction of CD in Figure 5.9 we encounter an ice-cream cone diagram, and hence we expect $L^{\oplus}(T_2)$ and $L^{\oplus}$("the diagram in Figure 5.12") touch near the pinch point in

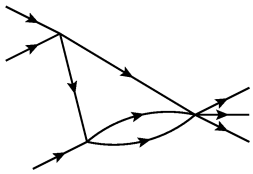

Figure 5.12. The ice-cream cone diagram.

question. This is really the case as show in Figure 5.13 below.

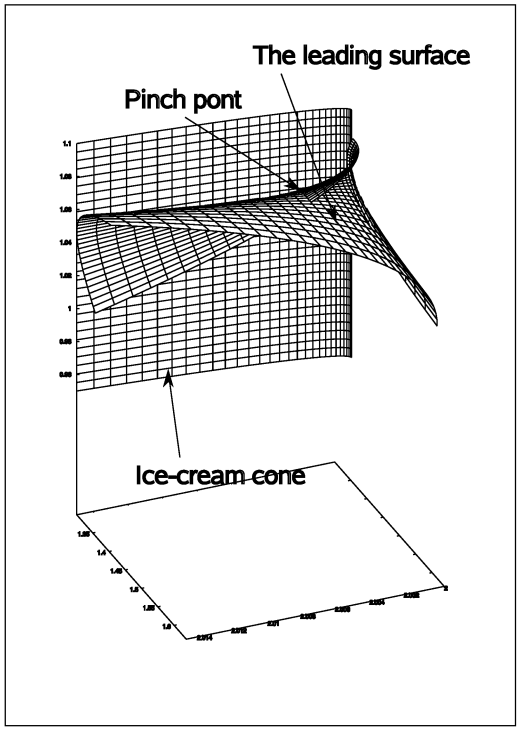

Figure 5.13.

On the other hand, $F_{T_2}(p)$, the Feynman integral associated with T_2 is well-defined near the intersection of the closure of $L^{\oplus}(T_2)$ and $L^{\oplus}$("the diagram in Figure 5.12") as

a microfunction. (Cf. [11], [9].)

Now, is it possible to write it more explicitly without using the integration procedure?

Remark 5.1. In conjunction with the above problem in microlocal analysis, we note that it seems not to be appropriate to mention ([8] p. 115) F_{T_2} as an possible example of applications of general theory of simple holonomic systems with non-singular characteristic variety; in fact the cusps observed in Figure 5.5 seem to be wilder than that expected in [8] p. 116. We plan to discuss this point in more detail in our future work.

To end this item concerning T_2, we show how the closure of $L^{\oplus}(T_2)$ intersects with $3PT$; as is expected outside N it cleanly intersect with $3PT$ along a submanifold of codimension 2 in the closure of $L^{\oplus}(T_2)$; the intersection is realized through the contraction of AB and DC in Figure 5.4. See the concrete figure shown in Figure 5.14.

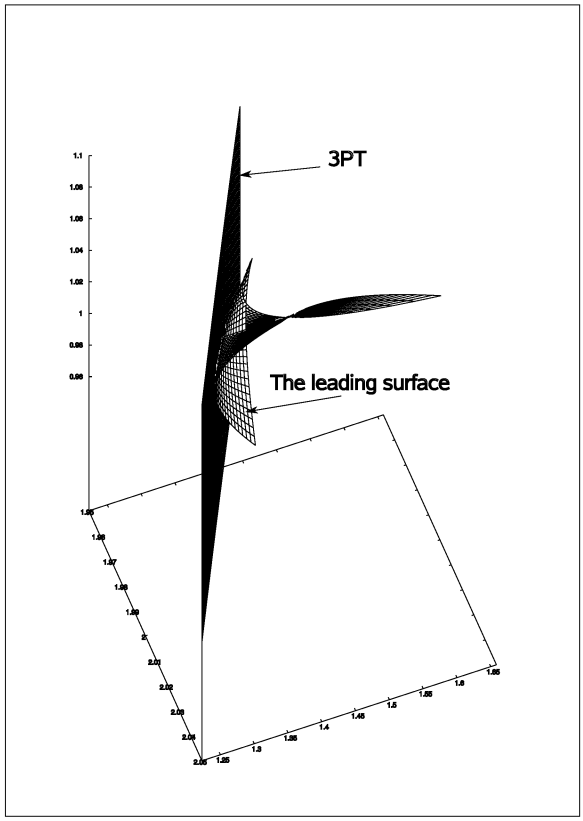

Figure 5.14.

[III] Finally let us study T_3. Although $L^{\times}(T_3)$ presents several interesting features, we concentrate our attention on its behavior near $3PT$. As some of the figures below are too complicated to grasp their details, we present in [5] some colored figures which may help the understanding of the reader.

Concerning the geometric feature of the leading LN surface $L^{\times}(T_3)$, the most remarkable one is the existence of codimension 2 component in $L^{\times}(T_3)$ (actually in $L^{\oplus}(T_3)$ as we see below). See also [4].

The relevance of the codimension 2 component and the codimension 1 component of $L^{\times}(T_3)$ is seen in Figure 5.15 below. Here we show the figure away from N. See Appendix B and [5] for the figure near N.

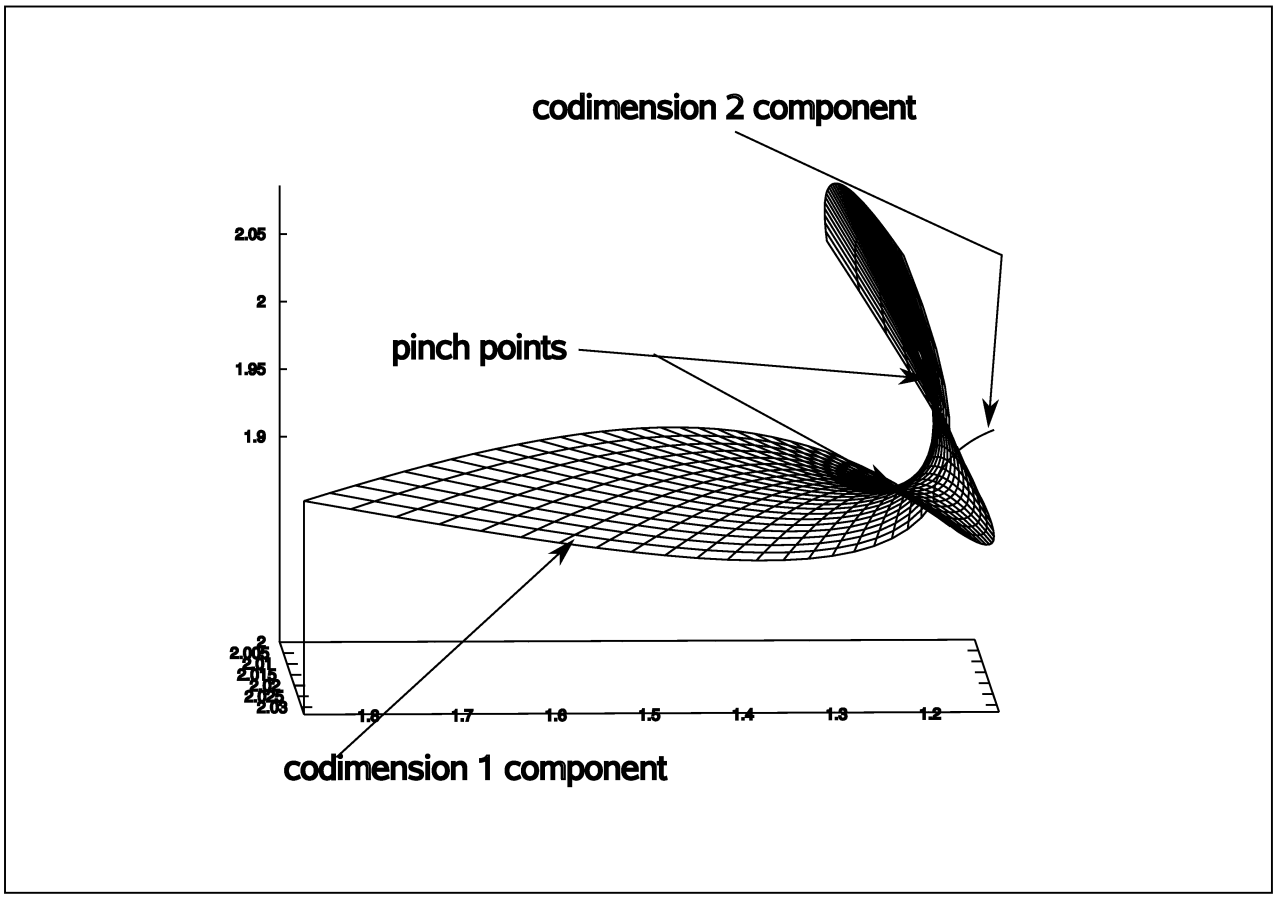

Figure 5.15.

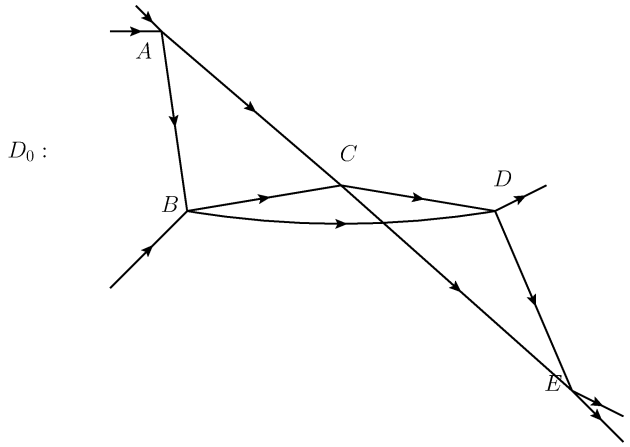

Figure 5.16. D_0.

As is observed in [4], the codimension 2 component is given by the following configuration D_0 in Figure 5.16. The flexibility of the vertex C indicates that

$$L^{\oplus}(D_0) \subset L^{\oplus}(I_L) \cap L^{\oplus}(I_R) \tag{5.7}$$

should hold, where I_L is in Figure 5.17 and I_R is in Figure 5.18, and we can validate

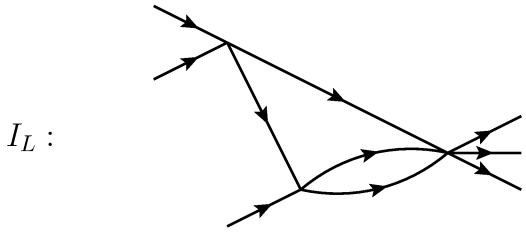

Figure 5.17. I_L.

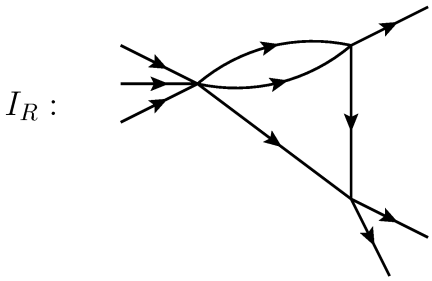

Figure 5.18. I_R.

(5.7) by the actual computation as shown in Figure 5.19.

Furthermore Figure 5.20 below shows how $L^{\oplus}(T_3)$, $L^{\oplus}(I_L)$, $L^{\oplus}(I_R)$ and $3PT$ are located outside N. We note that the cusps in $L^{\times}(T_3)$ do not appear in $L^{\oplus}(T_3)$. We also note, just in parallel with the case of $[L^{\oplus}(T_2)]$, that $[L^{\oplus}(T_3)]$ touches $3PT$ along a submanifold of $3PT$ with codimension 2, which corresponds to the simultaneous contraction of AB and DE. The intersection of $[L^{\oplus}(T_3)]$ and $3PT$ that corresponds to the contraction of the pair (BC, DE) or the pair (AB, CD) is not covered in Figure 5.20. The shape of $L^{\times}(T_3)$ and its relevance to $3PT$ are visualized in Appendix B and [5].

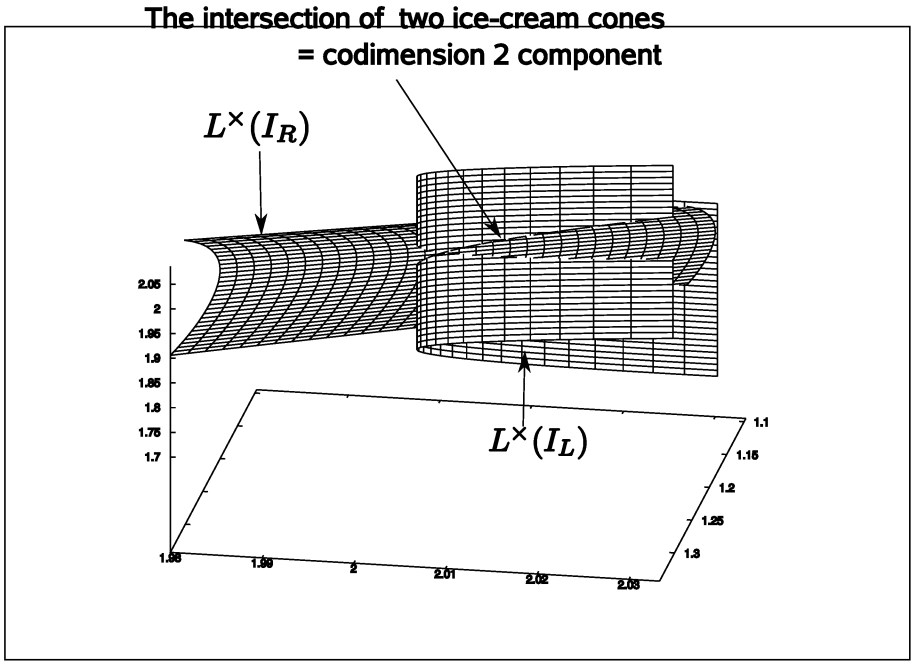

Figure 5.19.

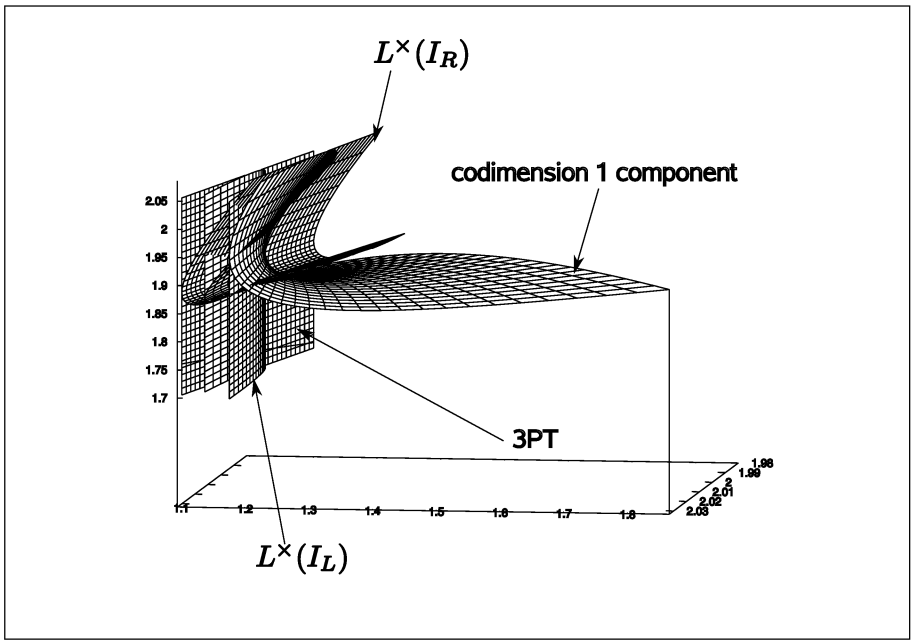

Figure 5.20.

§ 6. Future problems and concluding remarks

The obvious problem that remains to be done is to extend the results in this paper to the situation where the space-time dimension ν is 4. At this point we only point out that we need to study *hooked* 3-*twine diagrams* instead of hooked 3-lines diagram; it will remove the somewhat artificial impression on the definition of a hooked 3-lines where the middle line plays a special role; study of hooked 3-twine diagrams will enable us to study diagrams of the form in Figure 6.1 for example.

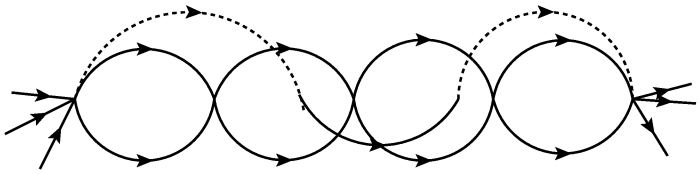

Figure 6.1.

Such an extension is certainly important and interesting, still we think we had better first deepen our analysis in the 2-dimensional case. The reason is as follows: since we are primarily concerned with the finiteness problem near $3PT$, we have not fully discussed in this article the geometrically interesting problem related to pinch points and cusps. At the same time, cusps appear in mixed-α (i.e., not necessarily positive-α) LN surfaces and they play important roles in studying the bubble diagram functions, a basic objects in analytic S-matrix theory. (See [9], [10] and references cited therein.) Furthermore our experience strongly indicates that better understanding of cusps should be important in analyzing the holonomic structure of Feynman integrals and the S-matrix. We also believe that some systematic understanding of pinch points and acnodes should be mathematically important and charming problem. The background of this belief is explained in Appendix A. Although the result there is, from the mathematical viewpoint, an elementary one, we believe no explanation of the origin of acnodes has ever been given at least in the literature of the S-matrix theory. Thus we see so many important and intriguing geometric problems remain in the study of LN surfaces even when the space-time dimension is 2. Further, the study of holonomic structure of Feynman integrals and the S-matrix has not yet been begun in this paper. We hope our geometric study in this paper will become a nice starting point of such analysis.

In this context we note that the study of holonomic systems with higher multiplicities is particularly important in rectifying Sato's postulates, which assume that relevant holonomic systems are simple ([11]). The estimation of the multiplicities of holonomic systems involved would lead to some tameness, other than holonomicity, of the singularity structure of the S-matrix even near m-particle threshold ($m \geq 3$) if we

could appropriately combine the result with the Borel summability of the perturbation series expansion of the S-matrix in the coupling constant. At this point we dare say also that it should be an interesting problem to study the Borel summability, or even the Borel transformability, of the perturbation series expansion of the S-matrix in energy-momentum space.

In ending this paper, we emphasize that the study of holonomic structure of individual Feynman integrals near N is an important problem, although our study in this paper is basically concerned with the points away from N. Concerning this point, we refer the reader to Appendix B where the concrete figure of $L^{\times}(T_3)$ near N is shown, together with $L^{\times}(I_L)$ and $L^{\times}(I_R)$.

§ Appendix A. Geometric study of $L^{\times}(T_1)$

The purpose of this appendix is twofold; first we want to show concretely how to visualize the leading LN surface $L^{\times}(T_1)$ with the help of a computer. The techniques shown below are equally applicable to the study $L^{\times}(T_2)$ etc. given in Section 5. Second we clarify why some complex singularities creep into the study of the singularity structure of Feynman integrals despite the fact that such singularities seem not to be anticipated from their behavior on the physical region. (Cf. [3] p. 106.) Although $L^{\times}(T_1)$ is basically irrelevant to $3PT$, its simplicity helps the reader to understand the core of the discussions in Section 5. Having these in mind, we include some elementary expositions here.

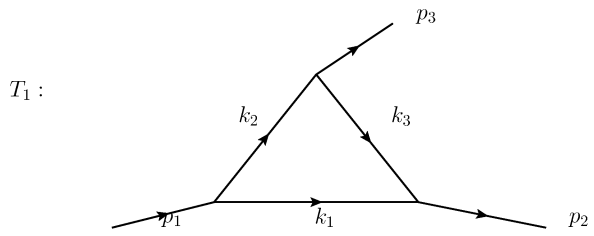

Figure A.1.

Our target is the diagram in Figure A.1 where all internal lines are attached with equal mass $m = 1$. In view of the over-all energy-momentum conservation law, the (leading) LN surface $L^{\times}(T_1)$ of T_1 is drawn in $\mathbb{R}^2_{p_1} \times \mathbb{R}^2_{p_2}$. We further employ the coordinate transformation of $\mathbb{R}^2_{(\tilde{p}_1,\tilde{p}_2)}$ to $\mathbb{R}^2_{(\tilde{x}_1,\tilde{x}_2)}$ given by

$$\tilde{x}_1 = \tilde{p}_0 + \tilde{p}_1, \quad \tilde{x}_2 = \tilde{p}_0 - \tilde{p}_1. \tag{A.1}$$

Thus the Minkowsky metric on $\mathbb{R}^2_{(\tilde{x}_1,\tilde{x}_2)}$ is given by

$$\tilde{x}_1\tilde{x}_2. \tag{A.2}$$

We may assume without loss of generality that

$$p_1 = (p,\, 0) \text{ with } p > 0. \tag{A.3}$$

Hence $L^{\times}(T_1)$ is described by 3 real variables (x, y, z) which satisfy

$$p_1 = (x,\, x), \quad p_2 = (y,\, z). \tag{A.4}$$

Since we are considering the problem in the 2-dimensional situation, the closed loop condition is satisfied for any triplet (k_1, k_2, k_3), if we set aside the positivity assumption

on the Landau constants α_ℓ's. Hence in view of the Minkowsky metric (A.2), we find that $L^\times(T_1)$ is described by the following relations with positive parameters $(s,\, t)$:

$$x = s + s^{-1}, \tag{A.5}$$

$$y = s + t, \tag{A.6}$$

$$z = s^{-1} + t^{-1}, \tag{A.7}$$

if we choose

$$k_1 = (s,\, s^{-1}), \quad k_2 = (s^{-1},\, s), \quad k_3 = (t,\, t^{-1}). \tag{A.8}$$

Then the computation (with a computer) gives us the following figure (Figure A.2).

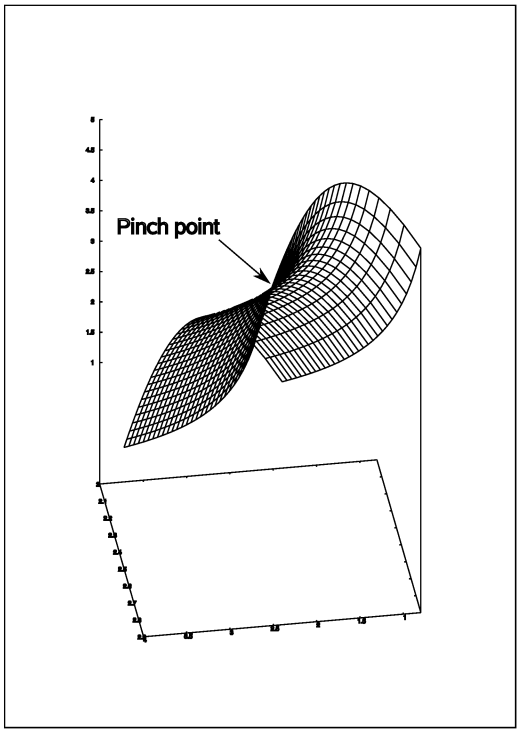

Figure A.2.

Furthermore the closed loop condition with positive α_ℓ's is met, barring the case where two k_ℓ's (and hence all k_ℓ's under the closed loop condition) are equal, if

$$s^{-1} < s < t, \text{ i.e., } 1 < s < t \tag{A.9}$$

or

$$t < s < s^{-1}, \text{ i.e., } 0 < t < s < 1. \tag{A.10}$$

Here we have compared the first component of k_ℓ's, having in mind their Minkowsky lengths are equal. Thus we find $L^{\oplus}(T_1)$ in the following Figure A.3.

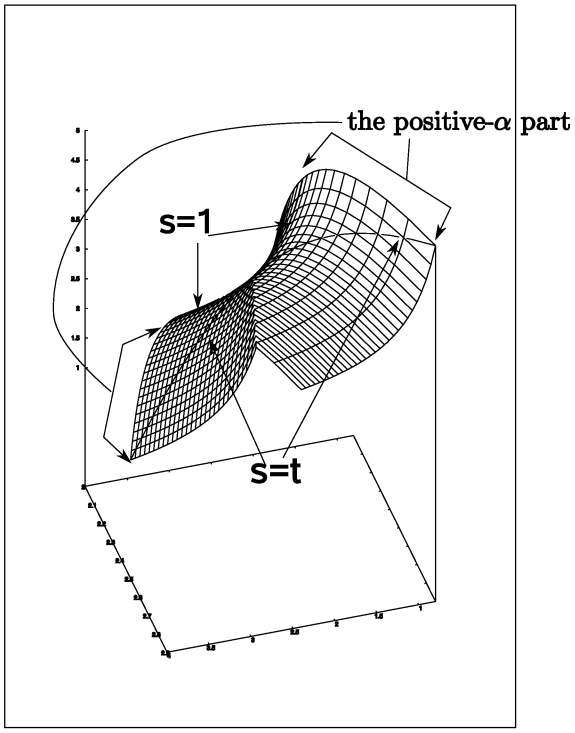

Figure A.3.

Thus there are no singular points in $L^{\oplus}(T_1)$ except for the pinch point; the pint point corresponds to the following configuration in Figure A.4, where $p_3 = 0$ and all k_ℓ's are equal.

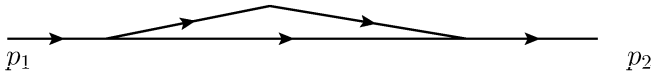

Figure A.4.

The cusp (i.e., self-intersection points) in $L^{\times}(T_1)$ is outside $L^{\oplus}(T_1)$. Thus, outside N, we do not observe any pathologies in $L^{\oplus}(T_1)$. At the same time Figure A.2 indicates that $L^{\times}(T_1)$ should be isomorphic to the so-called Whitney's umbrella W given by

$$X^2 = ZY^2, Z \geq 0. \tag{A.11}$$

It is really the case, and hence the "complexification" of $L^{\times}(T_1)$ requires some attention. Actually the complexification of some portion of Whitney's umbrella may be interpreted in either one of the following two interpretations:

(i) If we want to complexify W locally outside its pinch point (i.e., X=Y=Z= 0), i.e., if we consider a small complex neighborhood of w_0 ($\neq 0$) in W, then it suffices to extend W in the neighborhood; in this case, for example, the points where $X^2 = ZY^2$ with $Z < 0$ are irrelevant to the complexification if the neighborhood is sufficiently small.

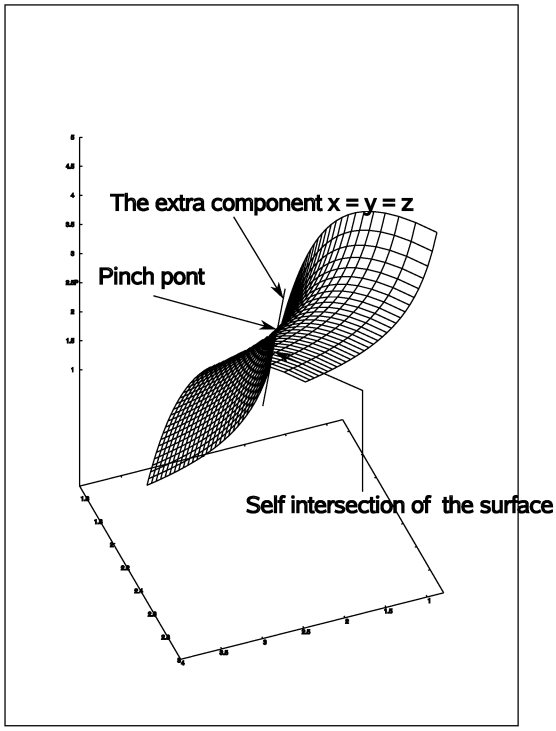

Figure A.5.

(ii) If we want to regard W as a complex variety defined globally, the points where $X^2 = ZY^2$ with $Z < 0$ are automatically contained in the complexification. Thus, if we use polynomials to define LN surfaces, as physicists usually do, then it means that we employ the standpoint (ii). Actually the cubic equation that Eden et al. use to describe $L^{\times}(T_1)$ (cf. [3] p. 62; (2.3.17)) assumes the following form in our variables (x, y, z):

$$(y - x)(z - x)yz + (z - y)^2 = 0. \tag{A.12}$$

Then the extra component $\{x = y = z\}$ appears in the real domain as is shown in Figure A.5. The appearance of this codimension 2 component in the real domain is a prototype of the acnodes in $L^{\times}(T_2)$ that was studied in detail in [3] and the references cited there, in conjunction with the Mandelstam representation.

§ Appendix B. Geometric study of $L^{\times}(T_3)$ near N

As we concentrate our attention on the geometric study of LN surfaces outside N in Section 5, we present here some instructive figures near N with some simple comments. The details will be discussed in [6]. We refer the reader to see [5] where some colored figures are shown.

First we show the following figure (Figure B.1) that shows the shape of $L^{\times}(T_3)$ near N.

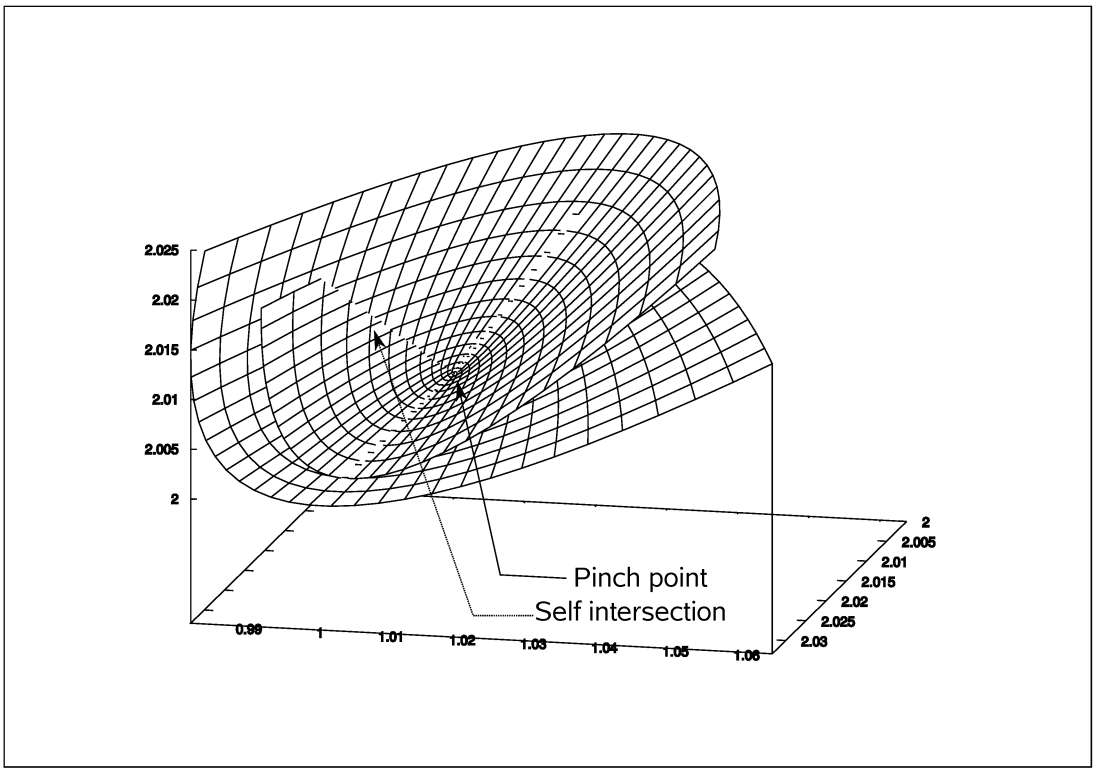

Figure B.1. The surface forms a double covering over a cone.

The following figure (Figure B.2) shows how $[L^{\times}(T_3)]$ touches with $3PT$. This makes a clear contrast to Figure 5.20.

In order to show how special the set N is we present Figure B.3 below, although it might be too complicated to decipher. We call the attention of the reader to the fact that $[L^{\times}(T_3)]$, $[L^{\times}(I_L)]$, $[L^{\times}(I_R)]$ all meet at N. Thus the set N is seen to be important in studying the holonomic structure of the individual Feynman integral, say F_{T_3}. We plan to discuss this point in more detail in [6].

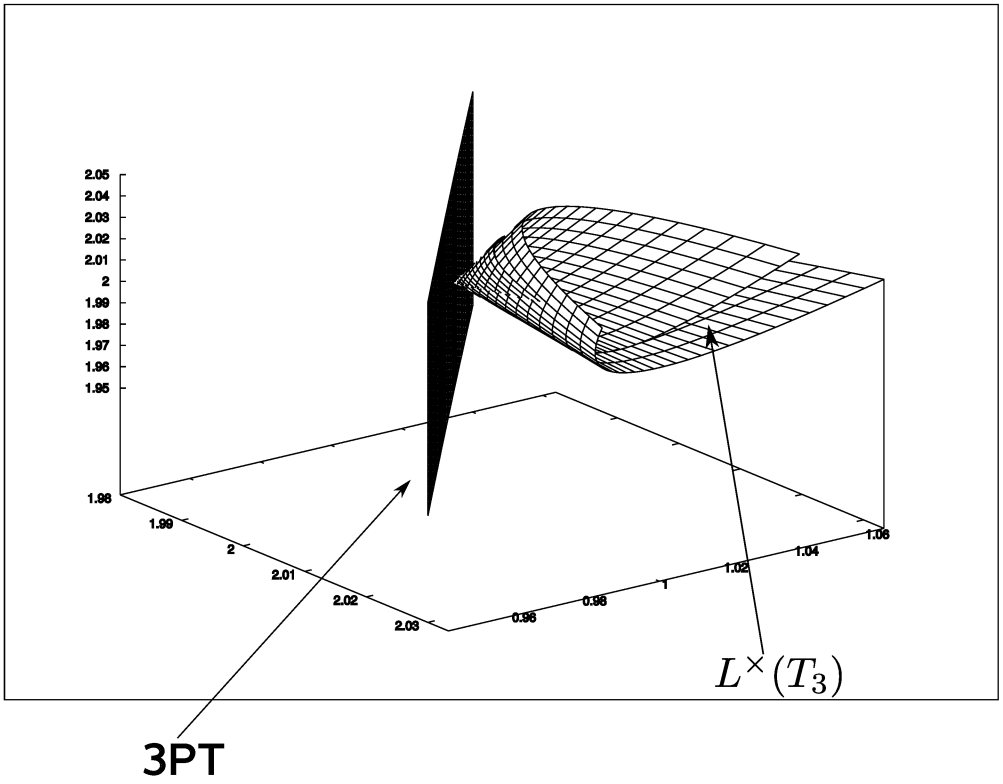

Figure B.2.

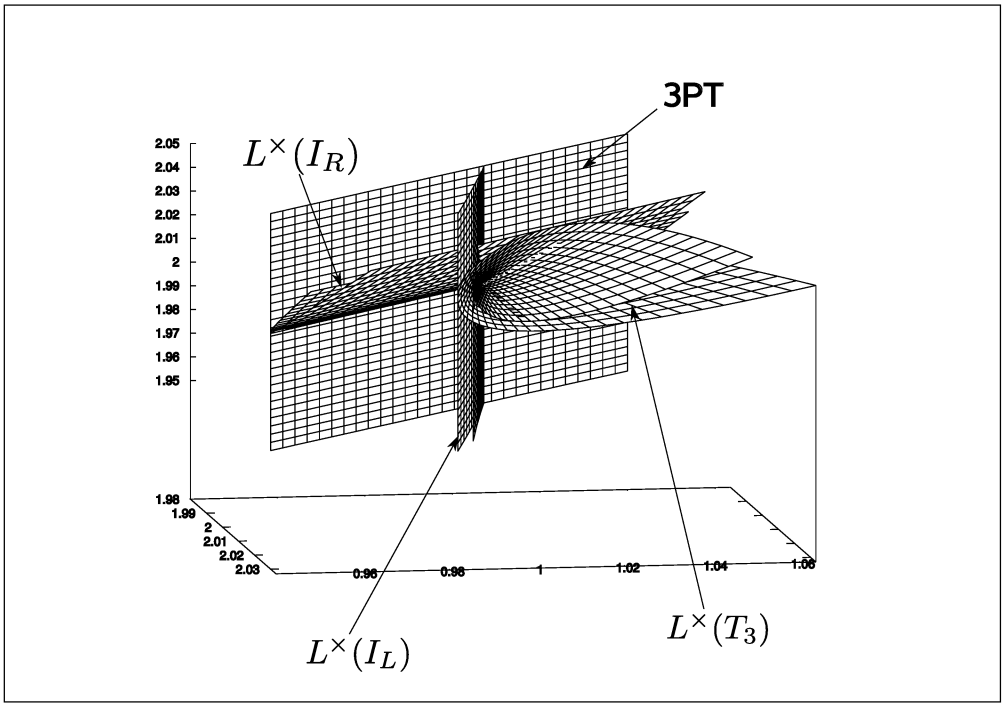

Figure B.3.

References

[1] C. Chandler and H. P. Stapp, Macroscopic causality conditions and properties of scattering amplitudes, *J. Math. Phys.*, **10** (1969), 826–859.

[2] J. P. Eckmann and H. Epstein, Borel summability of the mass and the S-matrix in φ^4 models, *Comm. Math. Phys*, **68** (1979), 245–258.

[3] R. J. Eden, P. V. Landshoff, D. I. Olive and J. C. Polkinghorne, The Analytic S-Matrix, Cambridge Univ. Press, (1966).

[4] N. Honda and T. Kawai, A computer-assisted study of the Landau-Nakanishi geometry. *RIMS Kôkyûroku* No.1861 (2013), 100–110.

[5] —, Visualization of the Landau-Nakanishi surfaces for truss-bridge graphs, RIMS preprint No. 1809 available at http://www.kurims.kyoto-u.ac.jp/preprint/index.html.

[6] —, A study of pinch points and cusps in the Landau-Nakanishi geometry, in preparation.

[7] D. Iagolnitzer and H. P. Stapp, Macroscopic causality and physical region analyticity in S-matrix theory, *Comm. Math. Phys*, **14** (1969), 15–55.

[8] M. Kashiwara, T. Kawai and T. Oshima, A study of Feynman integrals by micro-differential equations, *Comm. Math. Phys.*, **60** (1978), 97–130.

[9] T. Kawai and H. P. Stapp, Microlocal study of S-matrix singularity structure, *Lect. Notes in Phys.*, **39** (1975), Springer, 38–48.

[10] —, On the regular holonomic character of the S-matrix and microlocal analysis of unitarity-type integrals, *Comm. Math. Phys.*, **83** (1982), 213–242.

[11] M. Sato, Recent development in hyperfunction theory and its applications to physics, *Lect. Notes in Phys.*, **39** (1975), 13–29.